Gold Photocatalysis in Sustainable Hydrogen Peroxide Generation

Rohul H. Adnan[1]* and Aishah A. Jalil[2]

1. Nanoscience Lab, Faculty of Science, Universiti Teknologi Malaysia, 81310 Johor Bahru, Malaysia
2. School of Chemical and Energy Engineering, and Centre for Hydrogen Energy, Universiti Teknologi Malaysia, 81310 Johor Bahru, Malaysia

*Corresponding author: rohuladnan@gmail.com

Abstract

Hydrogen peroxide (H_2O_2) is a mild and green oxidant widely employed in organic syntheses, medical sector, disinfection, pulp bleaching, environmental remediation and biological processes. However, its production via the expensive, multiple steps and energy intensive anthraquinone process renders it less sustainable. Photocatalysis is a viable, sustainable and promising strategy to produce H_2O_2 from green sources: water and molecular O_2. This article presents key developments of photocatalytic H_2O_2 generation using gold (Au) nanoparticles supported on semiconductor photocatalysts. Several photocatalytic systems containing Au nanoparticles and the roles of Au nanoparticles in enhancing photocatalytic H_2O_2 generation including increasing the visible light absorption, facilitating the charge carrier separation and transfer, and as a catalytic active site are discussed. Factors defining the photocatalytic activity such as the effects of Au particle size and loading, localised surface plasmon resonance, mixed-gold component, and design of photocatalysts are reviewed. Finally, the challenges and prospect for further developments of Au photocatalysis in sustainable H_2O_2 synthesis as well as other related applications are highlighted.

Abbreviation

AQY	Apparent quantum yield
BiOBr	Bismuth oxybromide
$BiVO_4$	Bismuth vanadate
CB	Conduction band

CF	Carbon fibre
GQD	Graphene quantum dot
gC_3N_4	Graphitic carbon nitride
IET	Interfacial electron transfer
k_d	Rate constant of H_2O_2 decomposition
k_f	Rate constant of H_2O_2 formation
LDH	Layered double hydroxide
LSPR	Localised surface plasmon resonance
MoS_2	Molybdenum disulfide
MSI	Metal-support interaction
$NaBH_4$	Sodium borohydride
NR	Nanorod
NW	Nanowire
P25	TiO_2 with anatase (70-80%) and rutile (20-30%) phases
RGO	Reduced graphene oxide
$SrTiO_3$	Strontium titanate
TCPP	Tetrakis-(4-carboxyphenyl) porphyrin
VB	Valence band

1. Introduction

Hydrogen peroxide (H_2O_2) is a green oxidant which decomposes exothermically to water and molecular oxygen. The rate of decomposition of H_2O_2 can be controlled by its concentration, temperature, pH, and the presence of stabilizers or impurities. In an acidic medium, it forms a strong oxidant, more powerful than chlorine and potassium permanganate, such as piranha solution (in H_2SO_4) for cleaning glassware. The active oxygen content in H_2O_2 is 47 w/w% which makes it a desirable source of oxygen [1]. It is also a source of hydroxyl radical (•OH). As a result, H_2O_2 is commonly used in organic syntheses (e.g. olefin epoxidation, aromatic hydroxylation, alcohol oxidation), advanced oxidation process (e.g. Fenton process), bleaching, disinfection, and wastewater treatment [2]. More recently, in-situ production of H_2O_2 has been proposed as a convenient and portable fuel cell. An increasingly important role of H_2O_2 in biological processes includes wound healing and cell growth [3,4].

The most common, large-scale industrial production of H_2O_2 is the anthraquinone process. The process involves multiple steps: 1) hydrogenation of anthraquinone in the presence of a palladium (Pd) catalyst, 2) autooxidation of hydroquinone in the presence of air to produce H_2O_2 and regeneration of anthraquinone, 3) extraction of H_2O_2 from the solution through a separation column [5,6]. While the net reaction is simple ($H_2 + O_2 \rightarrow H_2O_2$), the process is expensive, tedious, and risky. The mixture of H_2 and O_2 entails a risk of explosion. The search for economical, safer, more efficient, and sustainable processes is crucial to meet the industrial demands and reduce environmental impacts.

Photocatalytic H_2O_2 production is a promising, safer and greener approach as compared to the traditional advanced oxidation process. Importantly, recent progress has shown feasibility of photocatalytic H_2O_2 production without the need of H_2 as a reactant which eliminates the risk of explosion. The synthesis of H_2O_2 from cheap, widely available water and O_2 is an ideal, desirable and promising alternative. Two key steps in a green, efficient generation of H_2O_2 are two-electron reduction of O_2 (step 3 in Figure 1) and water oxidation to H_2O_2 (step 7). Several possible steps of reduction and oxidation reactions involved as well as decomposition of H_2O_2 (step 4 and 5) are outlined in Figure 1 [7,8]:

Redox potential vs NHE

-0.33 V	1	$O_2 + e^- \rightarrow O_2^{\bullet-}$
-0.13 V	2	$O_2 + H^+ + e^- \rightarrow \bullet OOH$
0.68 V	3	$O_2 + 2H^+ + 2e^- \rightarrow H_2O_2$
0.87 V	4	$H_2O_2 + e^- \rightarrow \bullet OH + OH^-$
1.00 V	5	$H_2O_2 + h^+ \rightarrow O_2^{\bullet-} + 2H^+$
1.23 V	6	$2H_2O + 4h^+ \rightarrow O_2 + 4H^+$
1.76 V	7	$2H_2O + 2h^+ \rightarrow H_2O_2 + 2H^+$
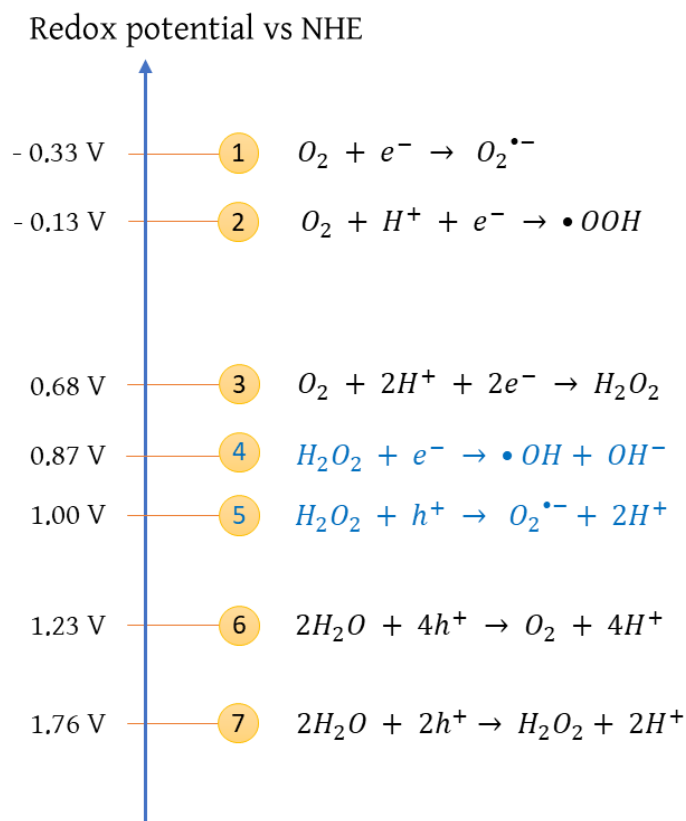
Figure 1. Redox potentials of some oxygen reduction and water oxidation reactions.

Here we provide a brief overview of the mechanism of H_2O_2 formation. From Figure 1, steps 3 and 7 are pathways towards H_2O_2 formation, namely two-electron oxygen reduction reaction (ORR) and water oxidation rection (WOR), respectively. Concerted direct two-electron reduction is thermodynamically feasible if the conduction band of photocatalysts is over +0.68 V vs NHE. Another pathway of ORR is two-step one-electron reduction, and it might compete with two-electron reduction when the conduction band is more negative than -0.33 V vs NHE [7]. However, this pathway may produce side reactions due to the highly reactive nature of radical species leading to reduced selectivity of H_2O_2 formation [9]. The two-step one-electron ORR pathway includes

$$O_2 + e^- \rightarrow O_2^{\bullet-} \tag{1}$$

$$O_2^{\bullet-} + H^+ \rightarrow \bullet OOH \tag{2}$$

$$\bullet OOH + H^+ + e^- \rightarrow H_2O_2 \tag{3}$$
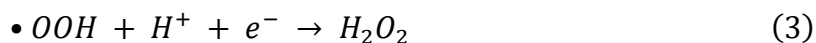
Although the WOR pathway is considered desirable since it requires water as the source of H_2O_2 and electron donor, the slow kinetics of WOR renders it the most unfavourable and difficult to achieve. In fact, alcohols or formic acid is often added to quench photogenerated holes as to prevent the electron-hole recombination. The WOR pathway can proceed via the following steps

$$H_2O + h^+ \rightarrow H^+ + OH^\bullet \tag{4}$$

$$OH^- + h^+ \rightarrow OH^\bullet \tag{5}$$

$$OH^\bullet + OH^\bullet \rightarrow H_2O_2 \tag{6}$$

Despite its promise, there are some issues associated with the photocatalytic of H_2O_2 generation. First, the sluggish kinetics of water oxidation causes a rapid recombination of photogenerated electron-hole pair. Second, the decomposition of formed H_2O_2 occurs in the reaction solution by the UV light irradiation, reaction with radicals/intermediates or photogenerated electrons or/and holes (step 4 and 5 in Figure 1) [10]. The yield of H_2O_2 production is governed by the competing rate constants of H_2O_2 formation (k_f) and decomposition (k_d). The k_f has been observed to follow the zero-order kinetics and the k_d is the first-order; the kinetics is described by the equation: $[H_2O_2] = (k_f/k_d)[1-\exp(-k_d t)]$. In principle, to obtain high H_2O_2 yields usually requires manipulating the reaction rates to maximise the k_f and minimise the k_d of H_2O_2 simultaneously.

Gold (Au) nanoparticle catalysts are highly active in a plethora of chemical reactions [11,12]. Hutchings's group has pioneered the use of gold catalysts in the synthesis of H_2O_2 from elemental O_2 and H_2 at low temperature [13,14]. Subsequently, Teranishi et al. demonstrated high yield of H_2O_2 (of millimolar order) in a photocatalytic reaction from O_2 and water using Au/TiO_2 photocatalysts under UV light [15]. The high photocatalytic activity was attributed to enhanced charge separation and spatial separation of oxidation (TiO_2 surface) and reduction (Au surface) sites. Another merit of incorporating Au nanoparticles is the visible light absorption due to the localised surface plasmon resonance (LSPR) that is beneficial for wide band gap semiconductors such as TiO_2, $SrTiO_3$, ZnO, and gC_3N_4. It has been demonstrated that an Au cathode in a photoelectrochemical cell was able to reduce O_2 to H_2O_2 under solar light irradiation without an applied bias [16].

Pristine semiconductor photocatalysts usually exhibit a high rate of charge carrier recombination and limited visible light absorption (for wide band gap materials) leading to low kinetics of H_2O_2 formation and low apparent quantum yield (AQY). Deposition of Au nanoparticles on the surface of photocatalysts brings about several benefits: 1) high selectivity for O_2 reduction to H_2O_2 compared to other metals (Pt, Pd, Ag), 2) enhancing charge carrier separation and transfer, 3) extending light absorption into the visible region, 4) behaving as a cocatalyst, and 5) modifying the surface chemistry of the photocatalyst. These factors contribute to many-fold increases in H_2O_2 production as compared to the pristine supports. For example, Au/WO_3 shows a 60-fold increase as compared to WO_3 [17] and Au/TiO_2 by 80-fold increase as compared to TiO_2 [18].

While there exists numerous reviews on Au plasmonic photocatalysts and Au photocatalysis in organic transformation and energy conversion [19–21], there is a lack of dedicated reviews on H_2O_2 production since the seminal work by Hiroaki Tada's group in 2010 [15]. Photocatalytic H_2O_2 production using supported Au nanoparticles is still at its infancy, and thus a review is necessary to provide the current status and recent progress in the field for newcomers and existing researchers. This review article presents the key developments and recent progress in the field in the last decade. The scope of this review is illustrated in Figure 2. We first describe preparation methods of gold photocatalysts. Next, factors contributing to high photocatalytic efficiency in H_2O_2 production such as Au loading and particle size, gold-mixed cocatalysts, photocatalytic supports, and the presence of additives will be discussed. In such discussion, various photocatalytic materials and designs containing Au nanoparticles will also be reviewed. A summary of photocatalytic performance of gold-

based photocatalysts in H_2O_2 generation is presented in Table 1. To close, we highlight challenges and prospect for future developments of Au photocatalysis in H_2O_2 generation and the related fields stemming from it such as advanced oxidation process, environmental remediation, photocatalytic oxidation and fuel cells.
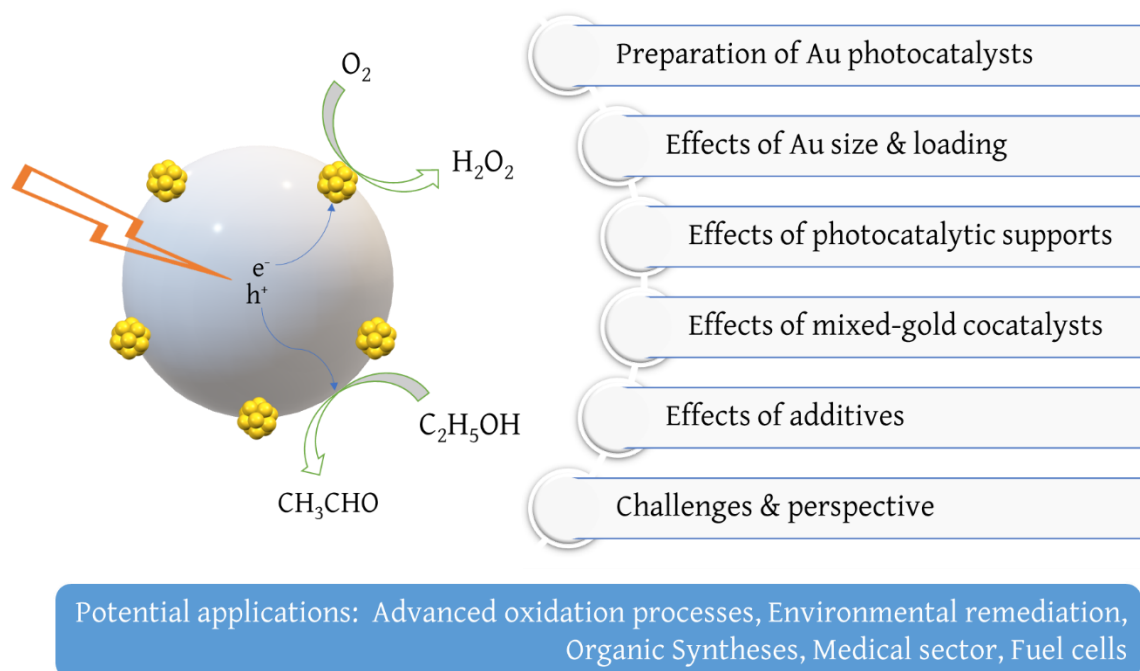
Figure 2. Illustration of the scope covered in this review

Table 1. Performance of Au-based photocatalysts in H_2O_2 production

Photocatalyst	Light source	Reaction solution	H_2O_2 yield	Time	AQY (%)	Ref.
0.25% Au/TiO$_2$	λ>300 nm	4% EtOH/water	~7 mM	24 h		[15]
0.25% Au/TiO$_2$	λ>300 nm	4% EtOH/water, pH 2, 5 °C	17 mM	23 h		[22]
0.88% Au/TiO$_2$-CO$_3^{2-}$	λ>430 nm	4% HCOOH/water, pH 1.7	1 mM	1 h	5.4% (530 nm)	[23]
0.61% Au/TiO$_2$	λ>320 nm	4% MeOH/water, phosphate, pH 9, 20 °C	1.39 mM	10 h		[24]
Au/TiO$_2$	367 nm	4% EtOH/water, 0.1M NaF, pH 3	59 μmol/mg	16 h		[25]
Au/TiO$_2$ porous film	UV 365 nm	5% EtOH in citrate buffer, pH 3.8	1 mM	5 min		[18]

Au/TiO$_2$/CF	λ>420 nm	4% HCOOH/water	2.9 mM	8 h		[26]
Au/TiO$_2$-F	Xe arc lamp	4% alcohol/water	~6.5 mM	12 h		[27]
0.35% Au/WO$_3$	λ>420 nm	4% CH$_3$OH/water H$_2$O	544 μM 177 μM	5 h 5 h		[17]
0.35% Au/WO$_3$	λ>420 nm	4% CH$_3$OH/water, Ni^{2+}	457 μM	5h		[28]
0.43% Au/ZnO	UV 365	4% EtOH/water	>1 mM	1 h		[29]
0.1% Au/ZnO	Xe lamp	4% EtOH/water, 0.1 M NaF	18.3 mM	12 h		[30]
0.5% Au/MoS$_2$	Xe lamp The sunlight	Water, pH 9, 10 °C	0.850 mM 0.792 mM	6 h		[31]
Au$_{0.2}$/BiVO$_4$	λ>420 nm	Water	40.2 μM	10 h	0.24% (420 nm)	[32]
Au/BiOBr	λ>420 nm	5% HCOOH/water	318 μM	2.5 h		[33]
0.01% Au/gC$_3$N$_4$	λ>420 nm	10% EtOH/water, pH 8.5	2.03 mM	30 h		[34]
2% Au/gC$_3$N$_4$	Xe lamp	5% IPA/water, pH 3	1.32 mM	4 h		[35]
Au/C$_3$N$_4$	λ>420 nm	9% IPA/water	990 μM	1 h		[36]
Au/N-GQD	Xe lamp	water	49.7 μmolg^{-1}h^{-1}			[37]
Au/BiVO$_4$-gC$_3$N$_4$	420 nm LED	Citrate buffer H$_2$O	1.35 mM 0.016 mM		6.7%	[38]
0.1% Au/Bi$_2$O$_3$-TiO$_2$	Xe arc lamp	4% EtOH/water	11.2 mM	12 h		[39]
0.32% Au/SnO$_2$(NR)-TiO$_2$	λ>430 nm	4% EtOH/water	~60 μM	6 h		[40]
Au/TiO$_2$-RuO$_2$	λ>300 nm	water	~80 μM	1 h		[41]
Au$_{0.1}$Ag$_{0.4}$/TiO$_2$	λ>280 nm	4% EtOH/H$_2$O	3.4 mM	12 h		[42]
Au$_{0.1}$Ag$_{0.2}$/ZnO	UV light	0.1 M MeOH	~1 mM	1.5 h		[43]
Cu@Au/BiVO$_4$	420 nm LED	5% MeOH/water	91.1 μM		0.88%	[44]
Au@CdS/gC$_3$N$_4$	λ=400- 780 nm)	10% EtOH/water	~65 μM	1 h		[45]
AuPd/BiVO$_4$	420 nm LED	0.2M citrate buffer, pH 3	2.29 mM	2 h	11.38	[46]
Si(NW)/Au/TiO$_2$ film	365 nm	water, ~pH 2	~40 μM	~25 h		[47]
Au/ZnO/TiO$_2$/Al film	λ>450 nm	5% EtOH/water	~0.45 μM	5 min		[48]
Au/ZnCr-LDH/RGO	Hg lamp	5% EtOH/water	24.3 μmol	2 h		[49]
Au-Co-TCPP	λ>280 nm	water	236 μM	1 h		[50]

2. Preparation of Au photocatalysts

Preparative methods of gold photocatalysts are highly influential to the photocatalytic performance. They give control over several parameters such as Au particle size, loading, dispersion, surface properties and metal-support interaction [51,52]. Importantly, photocatalytic designs also dictate the overall photocatalytic performance. Common methods include deposition-precipitation, co-precipitation, colloidal deposition, and photodeposition. Herein, we first provide a brief overview of preparation methods of gold photocatalysts.

The most common method to deposit Au nanoparticles on metal oxides including TiO_2, ZnO and $BiVO_4$ is deposition-precipitation (DP) initially developed by Haruta [29,32,53,54]. In this method, the pH of gold salt ($HAuCl_4$) is raised to be between 6 and 10 by urea or sodium hydroxide (NaOH) at elevated temperature to precipitate and deposit $Au(OH)_3$ on metal oxide supports. Calcination and chemical treatments are carried to reduce the gold precursors into metallic Au nanoparticles [55,56]. The advantages of this method are small size Au nanoparticles, narrow size distribution, and homogeneous dispersion of Au nanoparticles on supports. Tada and co-workers employed this method to produce highly active photocatalysts in H_2O_2 generation with controlled Au size from 2.1 to 12.5 nm by manipulating the calcination temperature and time [15]. This method is also effective for preparing mixed-gold cocatalysts using metal salt precursors.

Photodeposition (PD) has emerged as another effective method for immobilising Au nanoparticles on semiconductor photocatalysts. Typically, the gold salt precursor is added to a suspension consisting of a semiconductor photocatalyst. The suspension is irradiated with UV or visible light to excite electrons into the conduction band followed by reduction of the Au precursor and nucleation into Au nanoparticles. Advantages of this method are rapid formation of Au nanoparticles and selective deposition on edges, corners and particular facets of the support [57]. Recently, Shi et al. demonstrated selective deposition of Au nanoparticles on the electron-rich (010) facet of $BiVO_4$ which is favourable reduction of the Au precursor [38]. A comparison study between DP and PD by Li et al. found that the latter promoted more electron transfer from TiO_2 to Au nanoparticles resulting in higher photocatalytic activity under visible light irradiation [58].

Chemical reduction is also a popular method to prepare supported gold photocatalysts. A common reducing agent used in synthesis of Au nanoparticles is borohydride (KBH_4 or

NaBH$_4$). Due to strong reducing ability of borohydrides, ultrasmall Au nanoparticles (1-3 nm) are usually formed on supports [34]. The method proceeds conveniently at room temperature and does not require further calcination. Song et al. prepared Au/MoS$_2$ photocatalysts by reducing HAuCl$_4$ with a NaBH$_4$ solution in the presence of MoS$_2$ nanosheets [31]. Interestingly, the authors observed that two types of Au species, single atoms and clusters with less than 1 nm, are widely distributed on the surface of MoS$_2$ nanosheets (Figure 3).
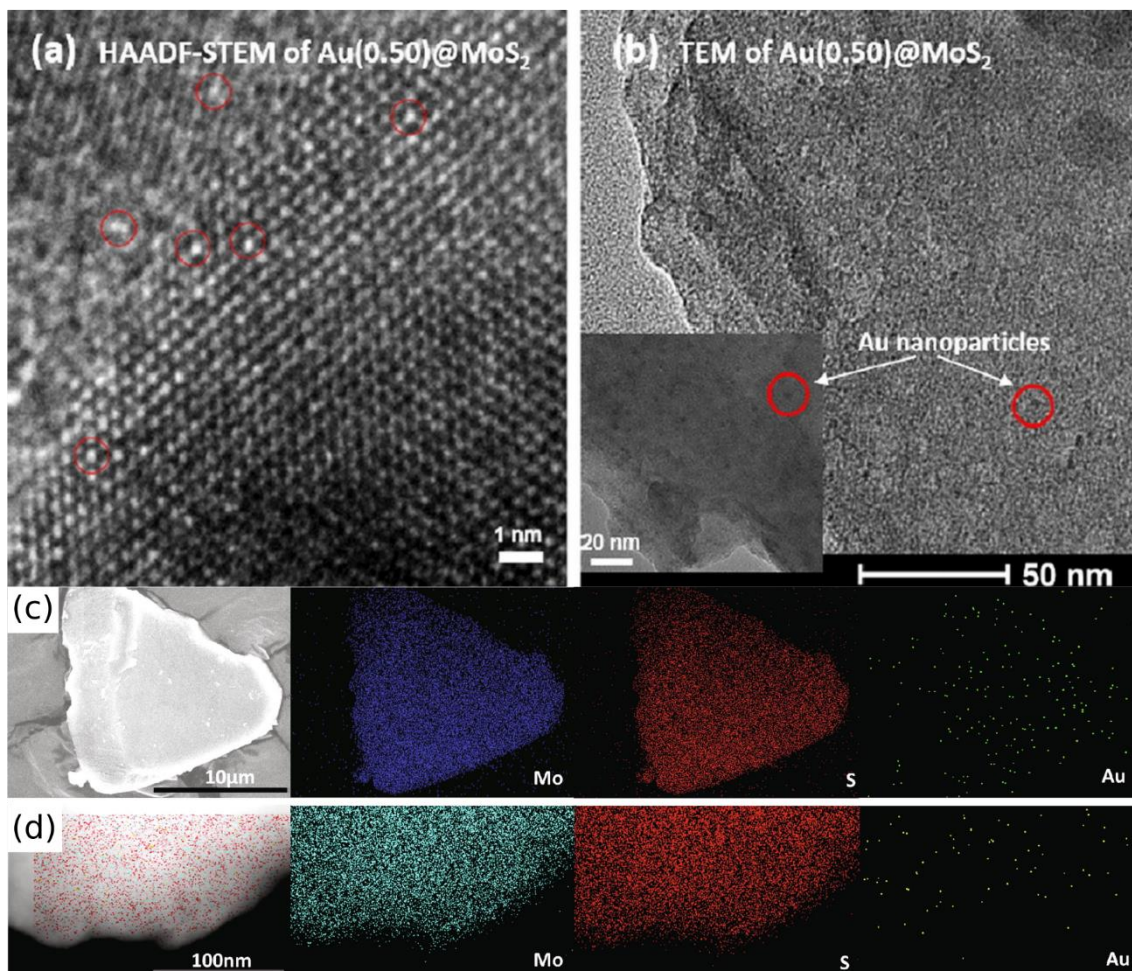
Figure 3. Images of 0.5% Au/MoS$_2$ showing the presence of (a) Au single atoms (in red circles), and (b) Au nanoparticles. Elemental mapping of 0.5% Au/MoS$_2$ using (c) SEM, and (d) TEM. Adapted from Ref. [31]. Copyright 2019, Elsevier.

For ligand-protected Au clusters, immobilization of the pre-formed clusters can be carried out by mixing a Au cluster solution in organic solvents such as dichloromethane or methanol with the support suspension, as illustrated in Figure 4 [59–62]. The key idea is to

manipulate the electrostatic interaction between ligands and the support. The simplicity of this method also allows deposition of ligated Au clusters on thin films by dip-coating the film in the Au cluster solution [63,64]. An advantage of this method is the control over the Au size against aggregation.
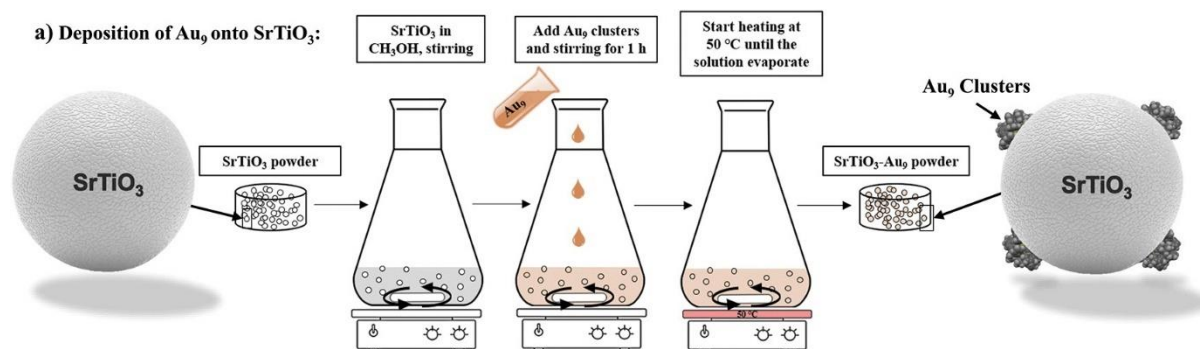

Figure 4. Schematic illustration of solution immobilisation of ligand-protected Au9 clusters on the SrTiO$_3$ support. Adapted from Ref. [62]. Copyright 2022, Royal Society of Chemistry.

3. Effects of Au particle size and loading

TiO$_2$ as of the most highly studied photocatalysts has severe drawbacks in photocatalytic H$_2$O$_2$ synthesis such as fast recombination of photogenerated electrons and holes, limited visible light absorption and decomposition of H$_2$O$_2$ [65]. Loading of Au nanoparticles on TiO$_2$ photocatalytic systems could reduce the decomposition of H$_2$O$_2$ on TiO$_2$ but unfortunately may directly decompose it to $^-$OH and •OH by the accumulated electrons in Au nanoparticles (step 4 in Figure 1). A few strategies have been conducted to suppress decomposition of H$_2$O$_2$ including probing the optimum Au size and loading, choosing suitable photocatalytic supports to regulate the charge transfer between Au nanoparticles and the support (refer to Section 4), and reducing strong adsorption of H$_2$O$_2$ on Au nanoparticles with mixed-Au metal cocatalysts (Section 5).

Teranishi et al. reported that when the Au size on TiO$_2$ was larger than 3.5 nm, the production yield of H$_2$O$_2$ increased as a function of the Au particle size [15]. The decreasing rate of H$_2$O$_2$ decomposition when increasing the Au size was attributed to the reduced number of catalytic active sites. Kawano et al. found that Au/ZnO exhibits much higher photocatalytic activity than Au/TiO$_2$ (Figure 5a). Likewise, a similar trend of size-dependent photocatalytic activity was also reported for Au/ZnO in following order: 4.9 < 6.0 < 6.6 < 9.8 nm Au size (Figure 5b) [29]. The k$_f$ of H$_2$O$_2$ increases gradually as the Au size increases but the

k_d of H_2O_2 decreases significantly (Figure 5c). In contrast, Au/WO$_3$ photocatalysts show a decrease in the photocatalytic activity as the Au size increases due to the increased plasmonic activity in H_2O_2 decomposition under visible light and lower interfacial contact between Au and WO$_3$ that stalls the photogenerated electron transfer [17].
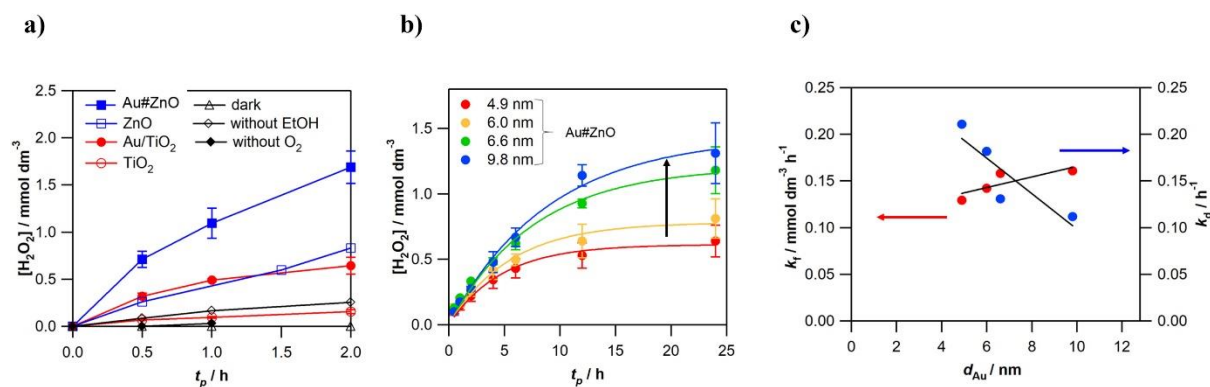
Figure 5. The concentration of H_2O_2 formation a) of different photocatalysts under different conditions, b) as a function of Au particle size in 4% ethanol aqueous solution, and c) plots of the rate constants for formation and decomposition of H_2O_2. Adapted from Ref. [29]. Copyright 2020, Elsevier.

Nevertheless, such a linear correlation is not always the case even in other similar photocatalytic systems. Often, a volcano-type (or inverse volcano-type) plot is found to describe the photocatalytic activity of Au catalysts where there is an optimum size for the highest photocatalytic activity [54]. For example, using Au/TiO$_2$ loaded on carbon fibre (CF) Xu et al. found that the optimum Au size of 5.3 nm gave the highest rate of H_2O_2 formation while smaller (2.3 nm) or larger (10.1 nm) Au nanoparticles are kinetically less active (Figure 6a-d) [26]. The broad size distribution of the 5.3 nm-Au/TiO$_2$ sample containing varying Au sizes was suggested to play a crucial role for high photocatalytic activity possibly due to size-dependent activity and population. Interestingly, this photocatalytic system exploits a triphasic interface where O_2 from air inside the porous carbon fibre can be directed to the solid photocatalyst to drive H_2O_2 generation in water (Figure 6e, f)[25,26]. Figure 6g shows that the production yield of H_2O_2 over 8 hours in a triphasic interface is three-fold higher (2.9 mM) than in a biphasic system (0.9 mM).

11
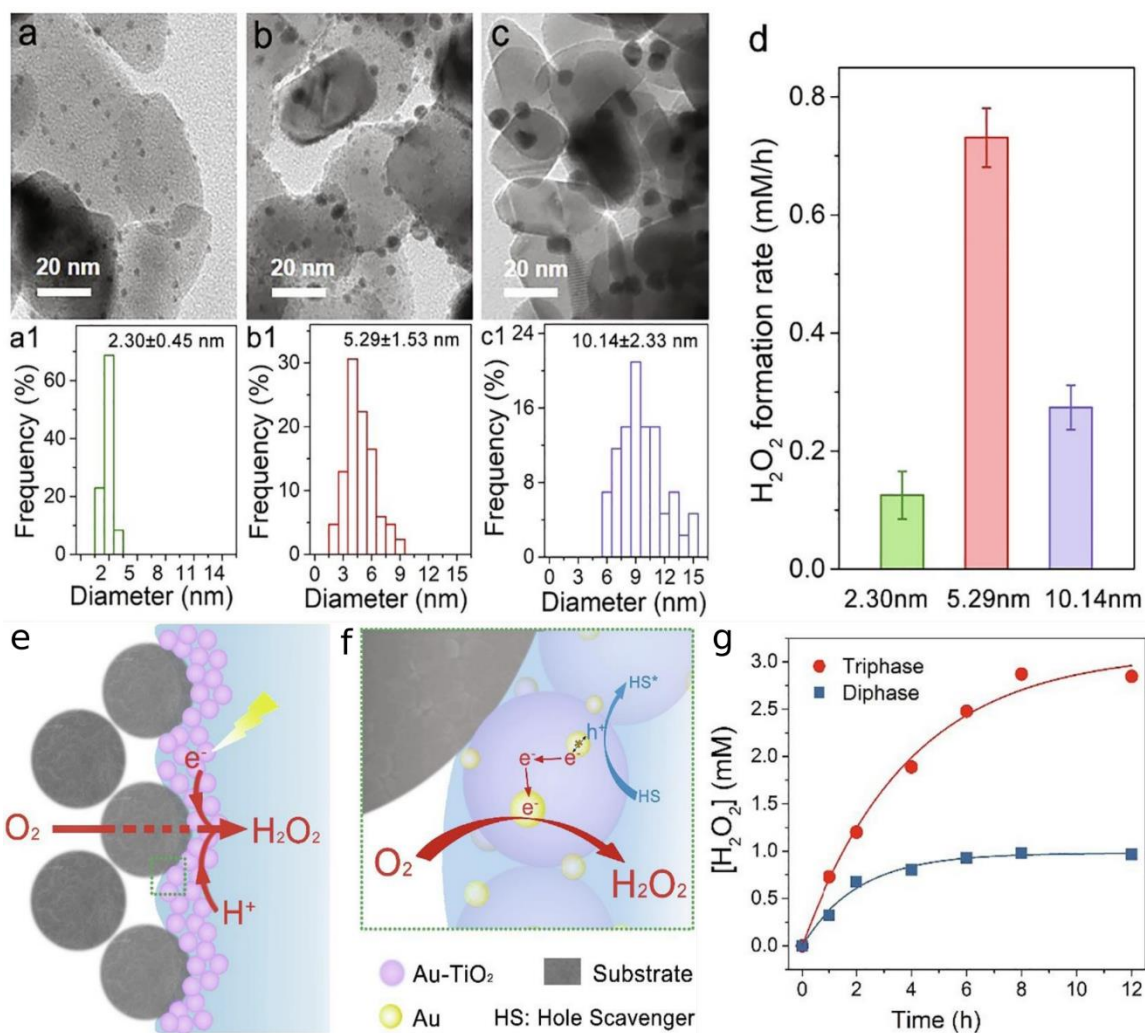
Figure 6. Size effect of Au nanoparticles supported on TiO_2 in photocatalytic H_2O_2 formation rate. Adapted from Ref. [26]. Copyright 2021, Elsevier.

More recently Kim et al. achieved a millimolar H_2O_2 production within 5 minutes using varying sizes (2-20 nm) of Au nanoislands on a porous TiO_2 film under UV light with an 80-fold increase compared to that of bare TiO_2 [18]. It has been shown that the work function of Au nanoparticles is size-dependent, and may dictate whether Au nanoparticles behave as an electron source or reservoir [66,67]. The authors reasoned that potential gradients are built at the Au-TiO_2-Au interfaces due to the size-dependent Au work functions leading to the efficient electron transfer across the Au(large)→TiO_2→Au(small) heterojunction (Figure 7a). In their work, small Au nanoparticles act as active sites to reduce O_2 to H_2O_2. Interestingly, the effects of bimodal Au size distribution on TiO_2 were also investigated by Naya et al. and proven to exhibit a superior photocatalytic performance than the individual unimodal photocatalysts [68]. Using photoelectrochemical measurements, it was found that, upon the

visible light illumination, the charge transfer proceeded from small Au to large Au nanoparticles via the CB of TiO_2 known as interfacial electron transfer (IET), illustrated in Figure 7b. As a result, small Au nanoparticles act as an oxidation site for water oxidation and large Au nanoparticles as a reduction site for O_2 reduction to H_2O_2 [23]. It can be seen that the role of Au nanoparticles either as the electron source or reservoir is highly dependent of the Au particle size, the LSPR effect, light wavelength and photocatalytic systems. It is therefore crucial to design photocatalysts with controlled Au particle size to maximize the rate and yield of H_2O_2 formation. The different role of Au nanoparticles in both works might be due to different photocatalytic designs *i.e.*, porous thin film vs powder.
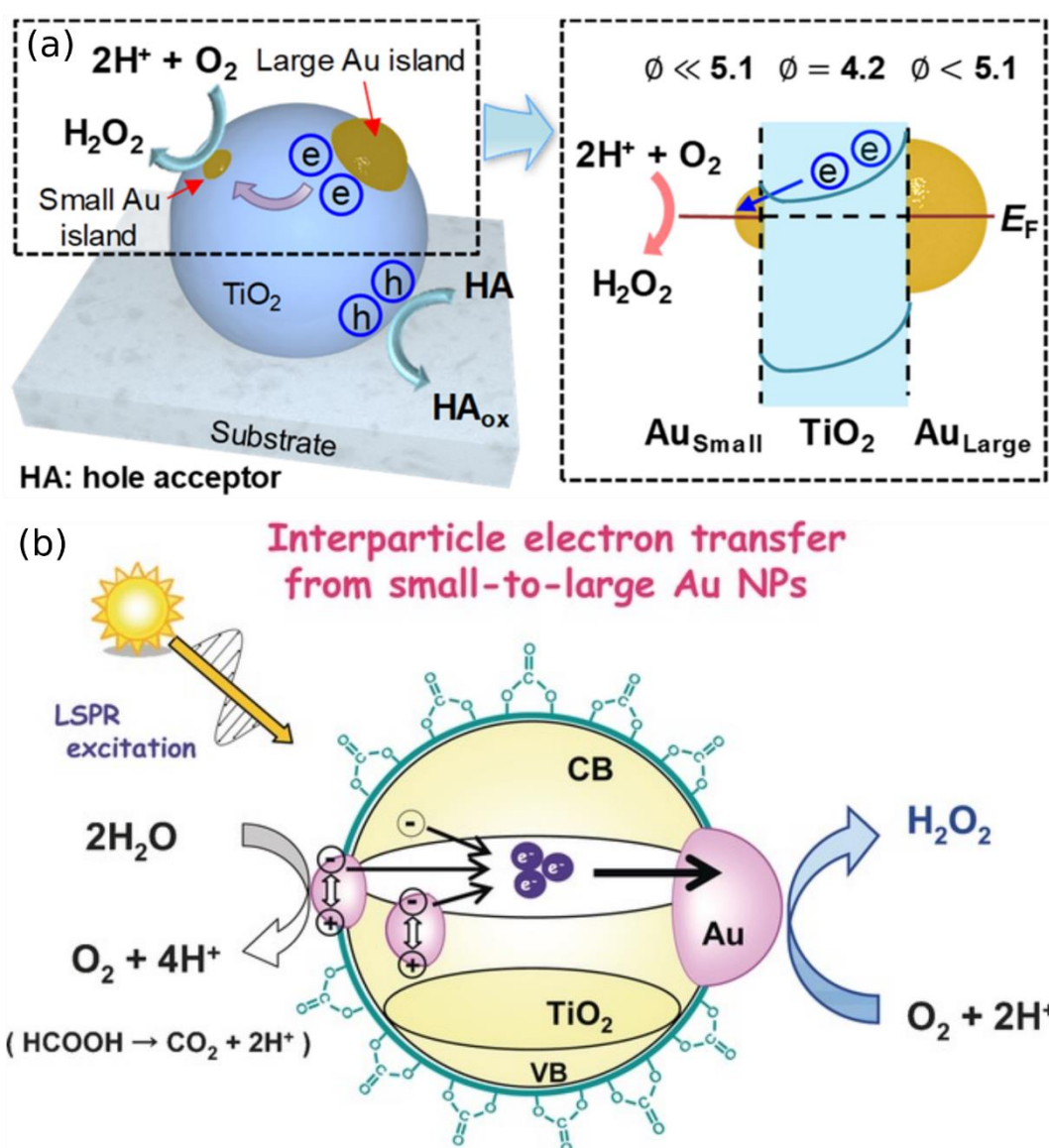
Figure 7. Illustration of electron transfer in (a) Au/TiO_2 porous thin film. Adapted from Ref. [18]. Copyright 2019, American Chemical Society. (b) Interfacial electron transfer from a

small to a large Au nanoparticle via the conduction band of TiO_2. Adapted from Ref. [23]. Copyright 2016, Wiley VCH.

For sustainable photocatalysis, it is desirable to reduce the material and process costs while maintaining high photocatalytic performance. While Au itself is a noble metal, its photocatalytic efficiency outperforms many other precious metals including Pt, Pd, and Ag nanoparticles [34]. Importantly, several works have demonstrated that a tiny amount of Au loading is required to achieve high yield and rate of H_2O_2 formation, usually much less than 1 wt% (refer to Table 1). Meng et al. suggested that the lower activity of 1% Au/ZnO as compared to 0.1% Au/ZnO is ascribed to the slow kinetics of H_2O_2 formation and blocking of light absorption in ZnO by a higher Au loading [30]. A similar observation was reported for Au/TiO_2 (P25) where a larger Au loading (>2 wt%) reduces the efficiency of catalytic sites [69]. Zuo et al. found that in Au/gC_3N_4 systems, the most active photocatalyst contained 0.01 wt% Au loading [34]. Surprisingly, almost no decomposition of H_2O_2 was observed in the 0.01% Au/gC_3N_4 over 12 hours. It could also be possible that higher Au loading causes aggregation which reduces the interfacial contact area between Au nanoparticles and the photocatalytic support thus reducing the photocatalytic activity.

The metal-support interaction (MSI) plays a defining role in many Au-based heterogeneous catalysts [70–73]. The perimeter interface between Au nanoparticles and the support is believed to be the catalytically active sites in many reactions [12]. In photocatalysis, a strong interfacial contact facilitates a charge transfer between Au nanoparticles and the photocatalytic support. Hirakawa et al. showed that similarly sized Au nanoparticles (~6.9 nm) but calcined at different temperatures (623 vs 673 K under air flow) exhibited a one-fold difference in the H_2O_2 formation yield [32]. The difference was attributed to the stronger degree of interfacial adhesion between Au and $BiVO_4$ at higher temperature which consequently improved the kinetics of photogenerated electron transfer. However, at larger temperatures severe aggregation occurs which dramatically reduces the number of active sites and catalytic activity.

Other calcination conditions (atmosphere, duration) influence the metal-support interaction which in turns affects the Au particle size, aggregation, and leaching. Chang et al. found that calcination of Au/gC_3N_4 under nitrogen (N_2) resulted in smaller Au sizes (5.0$\pm$2 nm), less agglomeration, reduced leaching, and gave a higher H_2O_2 yield (by +23.7%) as

compared to that of calcined under air [35]. It has also been observed that the influence of metal-supported interaction is more dominant than the Au size in many Au-based catalysts [74–76].

4. Effects of photocatalytic supports

Photocatalytic activity depends strongly on the type of photocatalytic supports. Apart from the position of the conduction band (CB) and valence band (VB) that are suitable for the redox potentials for H_2O_2 formation, the choice of photocatalytic supports is very important to stabilize Au nanoparticles and form a strong contact structure between Au nanoparticles and the support. Additionally, the surface properties of photocatalysts such as isoelectronic point, acidity/basicity and complexation regulate the adsorption and degradation of intermediate and H_2O_2; surface modification by ions is described in section 6. Besides TiO_2, other photocatalysts such as $BiVO_4$, WO_3, ZnO, gC_3N_4 and MoS_2 are widely used in photocatalytic H_2O_2 production.

ZnO has a band gap (3.37 eV) and band position similar to that of TiO_2. Contrary to TiO_2, ZnO does not adsorb H_2O_2 thus leading to a high photoactivity in H_2O_2 generation. It was reported that Au/ZnO generated over 1 mM of H_2O_2 in 1 hour, an order of magnitude higher than Au/TiO_2 (Figure 2A) [29]. The apparent difference of photocatalytic activity was attributed to the reduced decomposition of H_2O_2 on Au/ZnO based on the H_2O_2 adsorption study. Similarly, Meng et al. showed an exceptionally high yield (18.3 mM) of H_2O_2 using Au/ZnO as compared to 1.9 mM over Au/TiO_2 [30]. However, the use UV light irradiation and dissolution of ZnO in aqueous solution limits the practical use of Au/ZnO photocatalysts.

Bismuth-based semiconductors have been investigated as visible light responsive photocatalysts. $BiVO_4$ is a promising photocatalyst with the CB of 0.03 V which is lower than the one-electron O_2 reduction to •OOH (-0.13 V) but higher than two-electron O_2 reduction (0.68 V) making it selectively forms H_2O_2 via two-electron reduction. However, bare $BiVO_4$ hardly forms H_2O_2 due to the lack of active sites, and therefore requires the use of cocatalysts e.g. Au, Pd, Pt nanoparticles. Loading 0.2% Au nanoparticles on $BiVO_4$ increases the formation of H_2O_2 in water to 40.2 μM under the visible light irradiation [32]. Upon excitation by the visible light, the photogenerated electrons from the CB of $BiVO_4$ migrate to Au nanoparticles which reduce O_2 to H_2O_2. A similar role of Au nanoparticles was reported in an oxygen vacancy rich Au/BiOBr photocatalyst under the visible light irradiation [33].

Many works on photocatalytic H_2O_2 production are usually performed in an acidic medium due to the favourable proton-coupled electron transfer and instability of H_2O_2 in basic media; only few studies under basic conditions have been reported using appropriate photocatalytic supports. A high photocatalytic activity (0.85 mM in 6 hours) was observed over Au/MoS_2 in a basic medium (pH 9) due to the hole oxidation of OH^- to •OH which eventually dimerized to generate H_2O_2 i.e., •OH + •OH → H_2O_2 [31]. Moreover, Au/MoS_2 generate a high yield of 0.792 mM H_2O_2 in 6 hours under the real sunlight in pure water which holds a great promise for a real-world application.

Carbonaceous materials like graphitic carbon nitride (gC_3N_4) and graphene quantum dot (GQD) are a promising class of photocatalytic materials owing to their low cost, tunable band gap and surface functionality. It was found recently that Au/gC_3N_4 produced a high H_2O_2 yield of ca. 2 mM in an alkaline (pH 8.5) medium [34]. In another work, small Au nanoparticles (~5 nm) were found to anchor strongly on gC_3N_4 resulting in less aggregation and leaching, and an excellent H_2O_2 yield of 1.32 mM in 4 hours in an acidic (pH 3) medium [35]. These findings suggest that gC_3N_4 might be a versatile photocatalytic support for H_2O_2 generation across all pH with adjustable surface properties. Recently, Jiang et al. reported that an efficient electron transfer from the N atom in C_3N_4 to Au nanoparticles was observed in graphene-like Au/C_3N_4 which gave a high production rate of H_2O_2 close to 1 mMh^{-1} [36].

Recently there is a growing interest in simultaneous generation of H_2 and H_2O_2 in photocatalytic water splitting i.e., $2H_2O → H_2 + H_2O_2$, due to the ease of membraneless separation, safe process, and immediate use of H_2O_2 as an oxidant in organic reactions [77–79]. Importantly, it provides green method for clean energy carriers through a solar-to-H_2/H_2O_2 conversion. Liang et al. recently synthesized a composite photocatalyst made up of nitrogen-doped GQD (N-GQD) and Au nanoparticles wrapped with a few layers of graphene (graphene@Au) for photocatalytic water splitting into H_2 and H_2O_2 [37]. Incorporation of graphene@Au into N-GQD reduces the charge carrier recombination as manifested by low photoluminescence and high photocurrent (Figure 8a, b). The formation rate of H_2 and H_2O_2 are 65.6 and 49.7 $\mu mol\ g^{-1}\ h^{-1}$, respectively (Figure 8c, d).
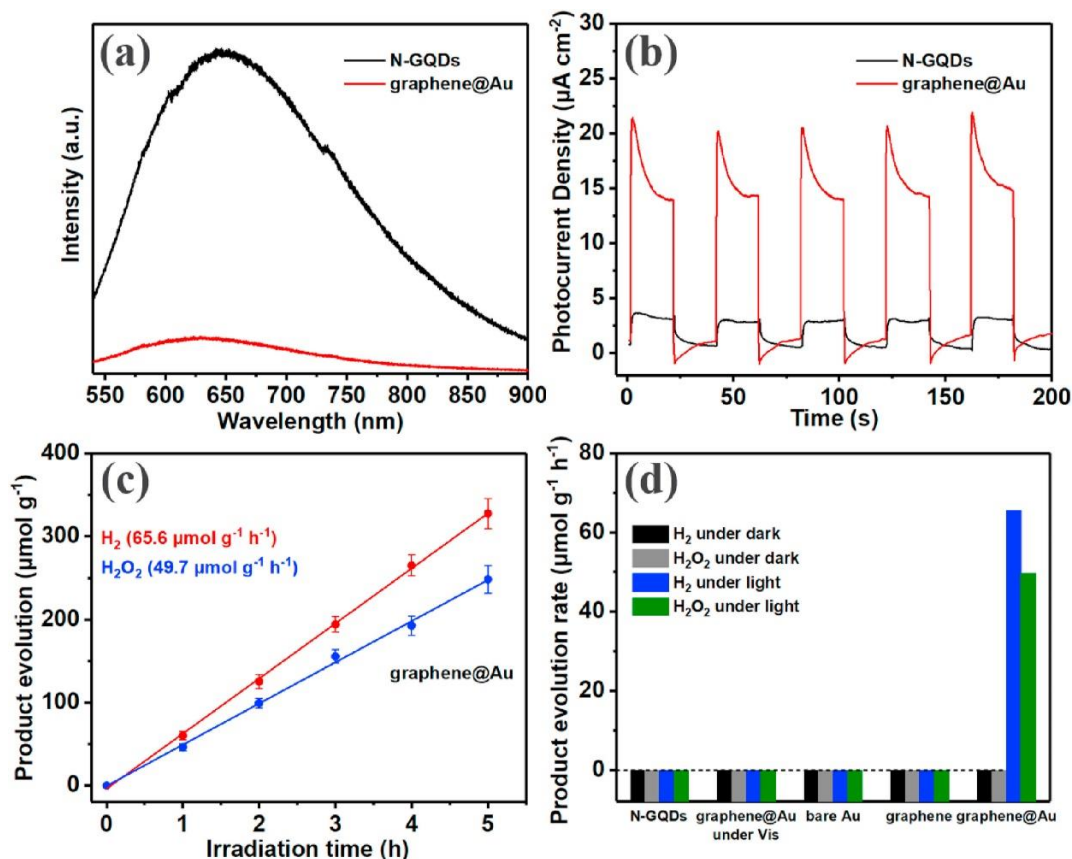
Figure 8. (a) Photoluminescence spectra, and (b) transient photocurrent response of N-GQD and graphene@Au/N-GQD. The formation (a) yield, and (b) rate of H_2 and H_2O_2 over N-GQD and graphene@Au/N-GQD. Adapted from Ref [37]. Copyright 2021, Elsevier.

In general, it is difficult to have a narrow band gap semiconductor and energetic redox potentials for H_2O_2 generation using a single component photocatalyst because such requirements are mutually exclusive. Thus, construction of heterojunction structures by coupling different semiconductor photocatalysts has been explored as a viable approach to design high-performance photocatalysts that exhibit superior photocatalytic efficiency than the corresponding individual photocatalysts.

Over $Au/BiVO_4$-gC_3N_4, the decomposition of H_2O_2 by photogenerated holes of $BiVO_4$ is suppressed by the efficient hole transfer to gC_3N_4 whereas the O_2 reduction proceeds on Au nanoparticles [38]. Besides the catalytic active site, Au nanoparticles can serve other roles thanks to the LSPR effect. In Au/CdS-gC_3N_4, the role of Au nanoparticles is to extend the visible light absorption range, CdS to provide the active site for O_2 reduction and gC_3N_4 to improve to photostability of CdS and enhance the charge transfer [45]. A similar role of Au

was found in Au nanoparticles loaded on ZnCr-layered double hydroxide and reduced graphe oxide (Au@ZnCr-LDH/RGO) by Mangsingh et al. [49]. Hot-electrons generated via the LSPR of Au nanoparticles accelerate the electron transfer to the CB of ZnCr-LDH and eventually to RGO where the O_2 reduction to H_2O_2 occurs.

Feng et al. developed a highly active three-component Au/Bi_2O_3-TiO_2 photocatalyst that afforded 11.2 mM H_2O_2 in 12 hours which was promoted by Au and Bi_2O_3 nanoparticles [39]. The author proposed that the photogenerated electrons from the CB of Bi_2O_3 migrated to Au nanoparticles, and holes to the VB of TiO_2 giving an effective charge carrier separation. Interestingly, the reaction mechanism was proposed to proceed via two-step one-electron reduction using in situ electron spin resonance (ESR) [39]. A similar observation was reported in Au/TiO_2-RuO_2 where the excited electrons in the CB of TiO_2 migrated to Au nanoparticles for O_2 reduction and holes transferred to the VB of RuO_2 [41]. Awa et al. recently designed a three-component Au/SnO_2(NR)-TiO_2 photocatalyst which showed a vectorial IET across Au(on TiO_2)→TiO_2→SnO_2→Au(on SnO_2) [40]. Interestingly, the reduction and oxidation sites in such system were identified to be Au nanoparticles on SnO_2 (A/SnO_2) and TiO_2 (Au/TiO_2), respectively.

Fabrication of thin film photocatalysts is appealing for controlling interface/surface properties using deposition methods such chemical vapour deposition (CVD), atomic layer deposition (ALD), epitaxial growth or sputtering. Kaynan et al. developed an Au/Si(NW)-TiO_2 film where Au clusters were embedded within the permeable TiO_2 shell giving a strong Au-TiO_2 interface that facilitated the charge transfer [47]. Such a film could also bring benefits in biological applications that require H_2O_2. Phillips et al. demonstrated that Au-sputtered Si NW films produced 6.2 $\mu M/cm^2$ H_2O_2 in 30 minutes in water under visible light and without any sacrificial agents suitable for intracellular H_2O_2 production [80]. However, the exact mechanism requires further studies, but it is believed the gold-silicon interface is responsible for the production of H_2O_2. Such finding could replace $Au/CdSe/CdS$ nanorod systems due to the concern of Cd toxicity [81].

One plausible approach to enhance light absorption and hot-electron lifetime of plasmonic Au nanoparticles is to confine electromagnetic fields by coupling with another metal. Willis et al. incorporated an Al film in an $Au/ZnO/TiO_2/Al$ stack (Figure 9a) to enhance the visible light absorption, hot-electron lifetime and the charge injection into the CB of ZnO thereby increasing the rate of H_2O_2 formation [48]. The presence of Al increases the visible

light absorption by coupling the light to Au nanoparticles leading to a 5-fold enhancement in light absorption and electron injection efficiency. Hot-electrons from the excitation of the LSPR of Au nanoparticles are injected into the CB of ZnO and subsequently reduce O_2 to H_2O_2 (Figure 9b, c). Figure 9d shows that the photocatalytic efficiency of the Al-incorporated device (Au-ZT-Al) supersedes that of non-Al device (Au-ZT-EXG) by more than three-orders of magnitude.
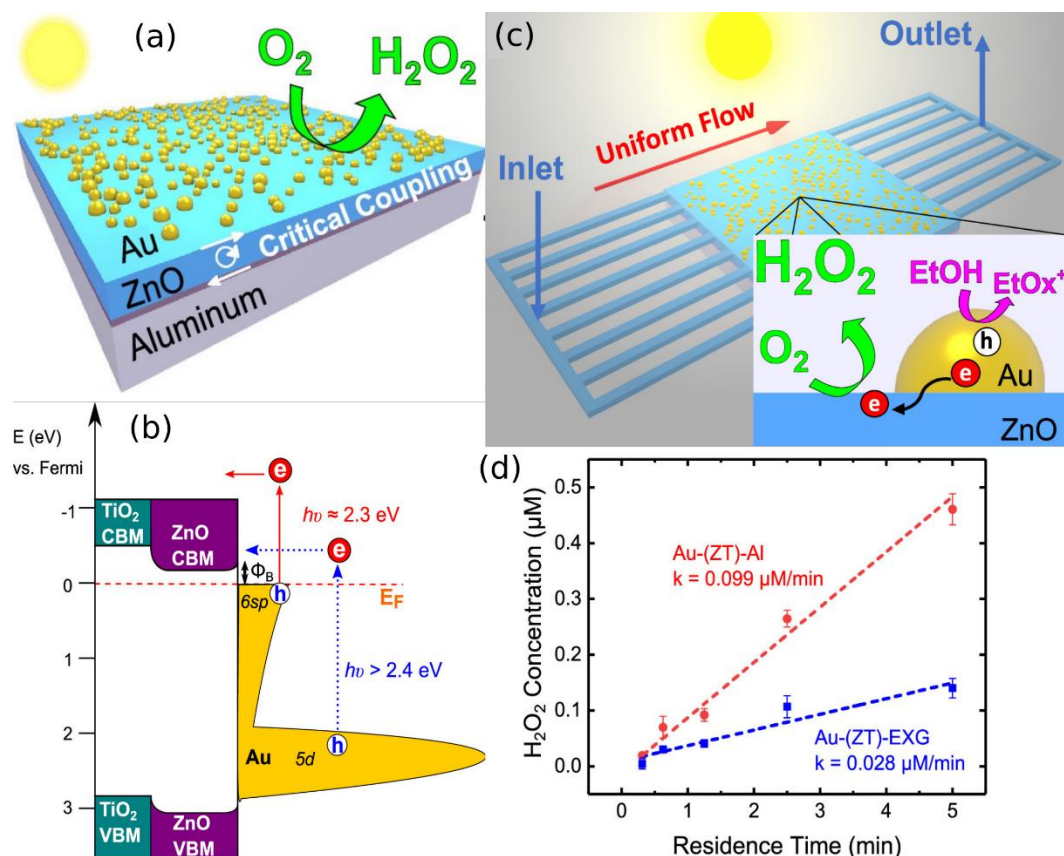

Figure 9. (a) Schematic diagram of the microreactor for in-situ H_2O_2 generation. The inset shows the active sites for O_2 reduction and ethanol oxidation. (b) Photocatalytic H_2O_2 yield with Al backing film (red) and without Al (blue). Adapted from Ref. [48]. Copyright 2020, American Chemical Society.

5. Mixed-gold metal components

The use of Au nanoparticles is more favourable than other noble metals (Pt, Pd, Ag) due to the higher activity and selectivity towards H_2O_2 formation. It has been found that the photocatalytic activity of metal supported on WO_3 followed the decreasing order: Au>Pd>Ag>Pt>Ni~Cu~Co [17]. Understanding the molecular interaction provides insights for

such high catalytic activity and selectivity. DFT calculations showed that the formation of H_2O_2 is more favourable over Au/TiO_2 (as compared to Pt/TiO_2) due to more favourable adsorption energy (-5.79 eV vs -4.76 eV for Pt/TiO_2) [82]. Importantly, it was found that the O-OH was not broken on Au/TiO_2 which led to a stable and selective formation of H_2O_2 whereas on Pt/TiO_2 the O-OH bond breaking occurred leading to the formation of water. This finding is consistent with other experimentally observed low yields of H_2O_2 formation on Pt/TiO_2 photocatalysts. Nevertheless, multimetallic cocatalysts might give unique catalytic activity due to the altered structure (alloy, core-shell), electronic and surface properties.

A strong H_2O_2 adsorption on Au nanoparticles often lead to its decomposition. This issue can be resolved by designing multimetallic cocatalysts containing Au and another metal to regulate the electronic structure and adsorption properties. Multimetallic cocatalysts are often employed to take advantage of the individual merits of every component, often called synergistic effect [83]. For example, Shi et al. exploited the high selectivity of two-electron O_2 reduction by Au and adsorption of O_2 by Pd to design an active and selective well-dispersed AuPd alloy nanoparticles on the electron-rich (010) facet of single crystal $BiVO_4$ [46]. The $AuPd/BiVO_4$ exhibits superior stability against H_2O_2 decomposition and higher activity (2.29 mM) than the corresponding $Au/BiVO_4$ (1.15 mM) and $Pd/BiVO_4$ (1.37 mM) as well as high reusability, as shown in Figure 10. Surprisingly, the high photocatalytic activity of $AuPd/BiVO_4$ was attributed to the well-dispersed Au and Pd atom distribution (compared to isolated Au and Pd atoms) in the AuPd alloy nanoparticles instead of the charge separation and transfer.
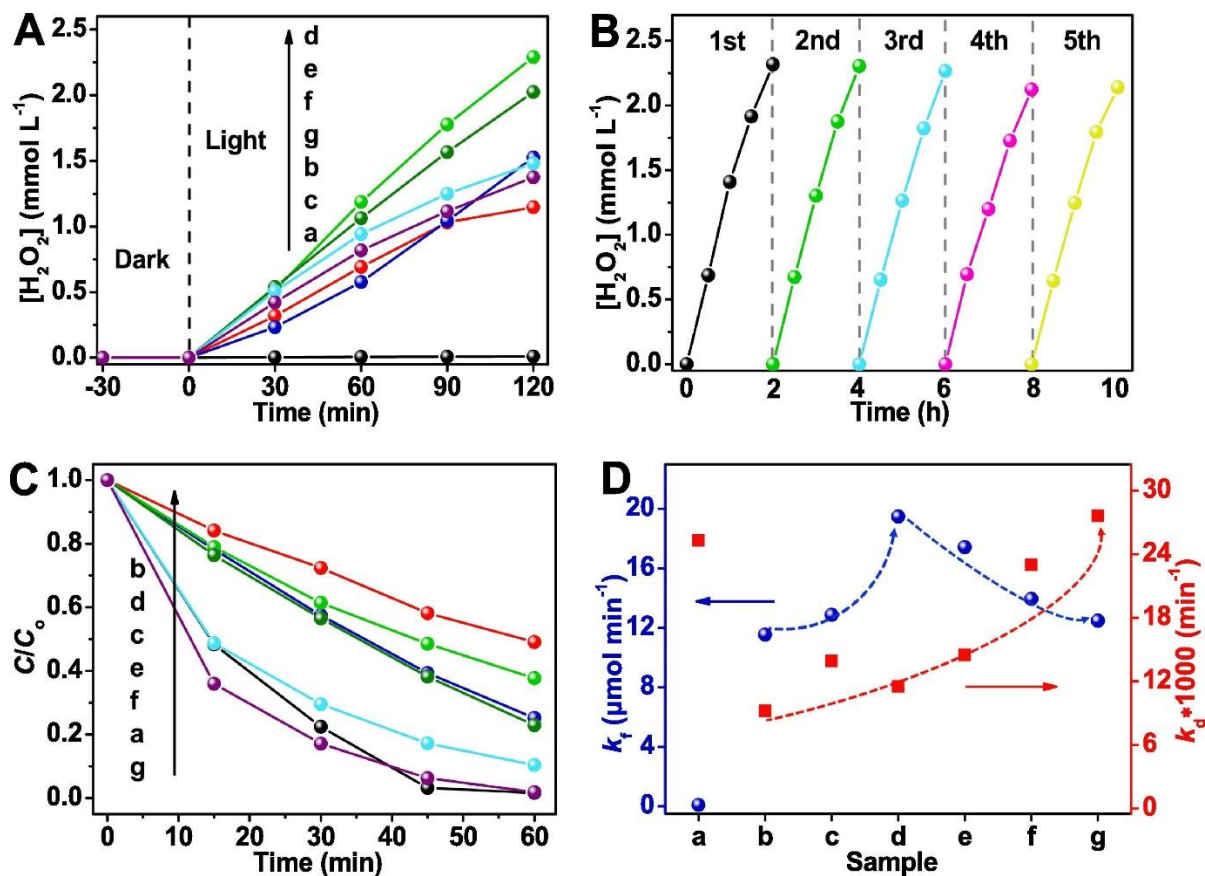
Figure 10. (A) Photocatalytic H_2O_2 production using various samples; (B) recycling test using AuPd/BiVO$_4$(010) (19:1); (C) photocatalytic H_2O_2 decomposition over time; (D) the k_f and k_d plots of various samples: (a) BiVO$_4$, (b) Au-BiVO$_4$(010), (c) AuPd/BiVO$_4$(010) (49:1), (d) AuPd/BiVO$_4$(010) (19:1), (e) AuPd/BiVO$_4$(010) (9:1), (f) AuPd/BiVO$_4$(010) (2:1) and (g) Pd/BiVO$_4$(010). Adapted from Ref. [46]. Copyright 2022, Elsevier.

Tsukamoto et al. compared the photocatalytic activity of 0.5 mol% metal loading of Au and Au$_x$Ag$_y$ nanoparticles; the subscripts x and y indicate the metal molar percentage. It was observed that while the rate constant of H_2O_2 formation (k_f) is quite similar for both Au$_{0.5}$/TiO$_2$ (0.53 mM h^{-1}) and Au$_{0.1}$Ag$_{0.4}$/TiO$_2$ (0.57 mM h^{-1}), the latter (0.14 h^{-1}) exhibits a lower rate constant of H_2O_2 decomposition (k_d) than the former (0.35 h^{-1}) [42]. The finding was attributed to reduced H_2O_2 adsorption by Ag in AuAg alloy thereby reducing its degradation rate. In other work, DFT calculations on a series of atomically-precise AuAg clusters supported on TiO$_2$ revealed the presence of mid-gap states in AuAg$_3$/TiO$_2$ and Au$_2$Ag$_2$/TiO$_2$ that are suitable for visible light absorption and H_2O_2 formation [84]. Recently, a core-shell Cu@Au/BiVO$_4$ nanostructure has shown an improvement in charge transfer mediated by the Cu core which

reduces an accumulation of negative charge on Au nanoparticles that is otherwise responsible for weaker adsorption of O_2 and HOO* as illustrated in Figure 11B and 11D [44].

Figure 11. A) The energy band diagram of $BiVO_4$, (B) Band bending and the charge density of $Au/BiVO_4$. (C) The volcano plot of Au positions of various samples in an oxygen reduction for the two-electron (blue) and four-electron (red) reductions, (D) Band bending in the $Cu@Au/BiVO_4$ photocatalyst design. Adapted from Ref [44]. Copyright 2021, American Chemical Society.

6. Effects of additives

In principle, the production of H_2O_2 from water oxidation and molecular O_2 reduction is an ideal, green process. Nonetheless, water and O_2 alone are not sufficient to give high apparent quantum yield of H_2O_2 formation due to the sluggish kinetics of water oxidation half-reaction which leads to a recombination of photogenerated holes and electrons. Two plausible approaches to circumvent this issue have been employed. First, addition of additives to alter the reaction conditions. Second, surface modification of photocatalysts to adjust the surface properties and acidity/basicity.

A little amount (within 5%) of alcohols - usually methanol, ethanol or isopropanol - are added as an electron donor or hole scavenger. Tert-butyl alcohol was found to perform less

efficiently than ethanol by three orders of magnitude [22]. Addition of benzylic alcohols boosts the formation of H_2O_2 up to 40 mM due to the formation of side-on peroxo species on TiO_2 from benzyl alcohols and O_2 in water that ultimately forms H_2O_2 [85]. Recently, furfuryl alcohol has been suggested as a promising hole scavenger in photocatalytic H_2O_2 formation [86]. Formic acid is also used as it serves a dual role to provide an acidic environment and electron donor. Milimolar orders of H_2O_2 yield have been achieved using formic acid on Au/TiO_2 photocatalysts[23,26].

An effective approach to reduce the rate of H_2O_2 decomposition via the reductive Ti-OOH pathway is to modify the surface of TiO_2 with other reagents. Complexation of the TiO_2 surface with fluoride ions (F^-) is known to inhibit the formation of peroxo/superoxo species [87]. However, too much fluoride ions will create defects and cause destruction of the crystallinity of TiO_2. Au modified $F-TiO_2$ was found to exhibit a four-fold increase in the H_2O_2 production as compared to Au/TiO_2 [27]. Additionally, NaF can be added to the reaction mixture as a source of F^- ions. Teranishi et al. observed that surface modified Au/TiO_2 with carbonate ions (CO_3^{2-}) enhanced the yield by more than one order of magnitude [23]. The chemisorbed CO_3^{2-} ions on TiO_2 hinder the decomposition of H_2O_2 that usually proceeds through the formation of Ti-OOH species.

The effects of addition of metal ions and inorganics anions to the reaction solution have also been reported. Ni^{2+} and F^- ions play both positive and negative roles in the presence and absence of methanol over the Au/WO_3 photocatalyst, respectively [28]. In the presence of methanol, Ni^{2+} and F^- facilitate methanol oxidation while in its absence, they prevent O_2 adsorption and reduction. Cu^{2+}, Fe^{3+} and Co^{2+} were found to catalyse decomposition of H_2O_2 and thereby decreasing the overall yield of H_2O_2 generation (Figure 12A). A further increase in the concentration of Ni^{2+} beyond 1 mM results in decreasing yield of H_2O_2 due to the absorption of light and inhibition of O_2 adsorption on Au photocatalysts by Ni^{2+} ions (Figure 12B). Wang et al. also found that PO_4^{3-}, CO_3^{2-} and SO_4^{2-} anions contributed greatly towards photocatalytic H2O2 generation where they scavenged the photogenerated hole (Figure 12C).
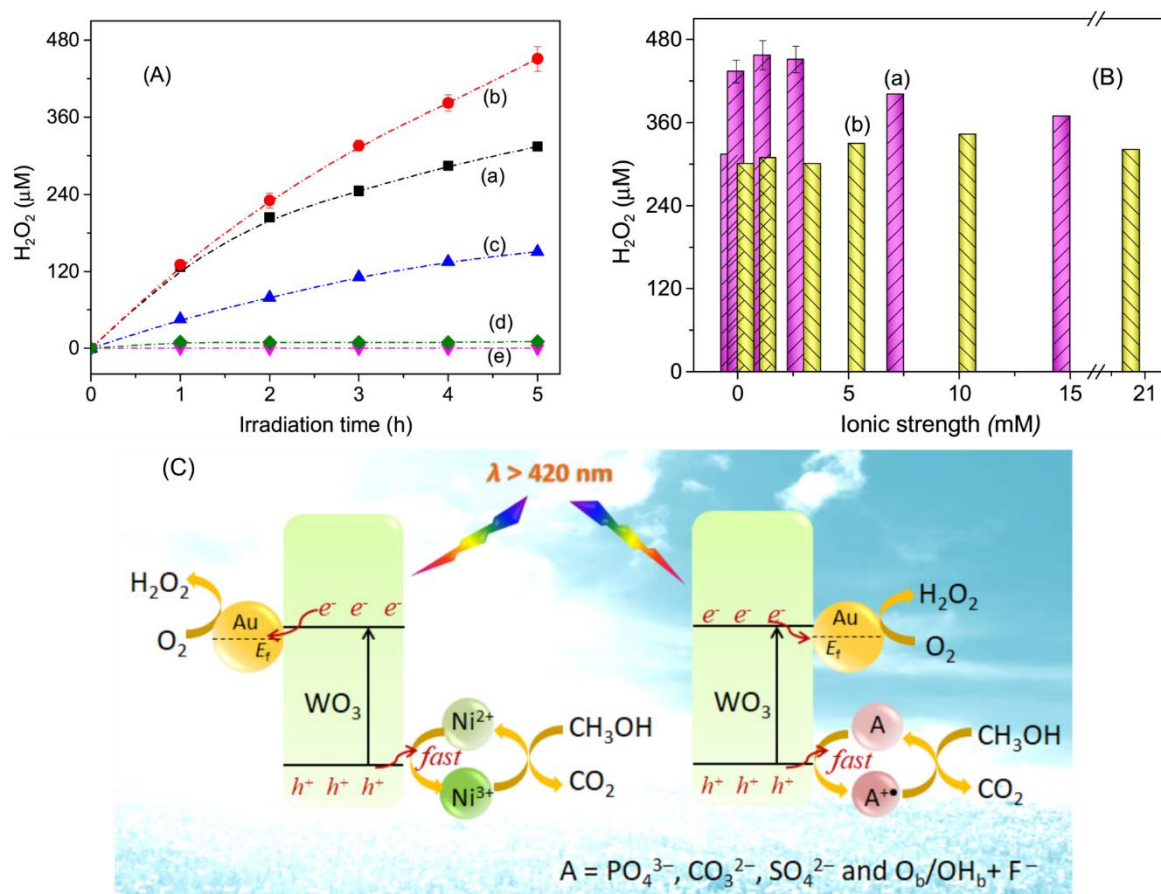
Figure 12. The H_2O_2 yield using Au/WO_3 as a function of (A) irradiated time for different cations: (a) no ions, (b) Ni^{2+}, (c) Co^{2+}, (d) Cu^{2+}, and (e) Fe^{3+}; and (B) ionic strength for (a) 0-5.0 mM Ni$(ClO_4)_2$ and (b) 0-20 mM $NaClO_4$. (C) The proposed mechanism of positive contribution of Ni^{2+} and selected anions. Adapted from Ref. [28]. Copyright 2021, Elsevier.

Synthesis of H_2O_2 in alkaline/basic media is challenging because of two reasons: H_2O_2 decomposes faster in alkaline media, and the formation of H_2O_2 in acidic media is facilitated by the proton-coupled oxygen reduction. As a result, many works reported high H_2O_2 production rate in acidic conditions (Table 1). However, Xiong et al. showed that high H_2O_2 up to 1.39 mM yield could be achieved at pH 9 using Au/TiO_2 with the addition of phosphate or borate ions [24]. Using photoelectrochemical measurements, their role was identified as to mediate the hole transfer that improves the charge separation.

7. Challenges and perspectives

Gold photocatalysis holds a promise for safe, green, economical and sustainable in-situ production of H_2O_2 with reduced environmental impacts and energy consumption as compared to the traditional, industrial anthraquinone process. Numerous works reviewed here highlight impressive performance that can afford up to millimolar H_2O_2 yields within several hours. Despite the potential, the current status and progress of Au photocatalysis in H_2O_2 production is still at its infancy, and immense effort and further research are needed to achieve the current performance of commercial H_2O_2 production.

While Au nanoparticles significantly increase H2O2 generation, it also unfortunately decomposes H_2O_2.

Progress of Au photocatalysis in H_2O_2 production is still fundamental in nature and at the lab-scale demonstration. The apparent quantum yields are low for many photocatalytic systems particularly in the visible light region. Some long-standing challenges that delay the practical application include:

1) low yield (usually micromolar) and formation rate of H_2O_2
2) rapid H_2O_2 decomposition
3) the use of UV light instead of visible light
4) long-hour photocatalytic reaction
5) reaction in pure water without any sacrificial agent

There are complex, competing factors that govern the photocatalytic activity of H_2O_2 production. The yield of H_2O_2 formation is primarily governed by the competing rates of formation and decomposition of H_2O_2. Both rates depend on many factors including the Au particle size, loading/coverage, and contact structure with the photocatalytic support. While the photocatalytic activity varies among photocatalytic systems, the findings discussed in this review article could serve as starting point for further research and developments. There exists general understanding for strategic designs of efficient supported Au photocatalysts. We summarize key points as the guidelines for developing high-performance Au photocatalysts in H_2O_2 generation.

1) **Contact structure at the perimeter interface**. A contact structure between Au nanoparticles and the support plays a few roles. First, a strong contact structure is favourable for enhanced charge transfer between Au nanoparticle and the

photocatalytic support. Second, it controls the aggregation and active sites of Au nanoparticles. Reducible metal oxides like TiO_2, ZnO and CeO_2 tends form a strong contact with Au nanoparticles owing to the metal-support interaction (MSI). Importantly, the contact structure is also influenced by the deposition methods and calcination conditions.

2) **Control of Au size and loading**. Size-dependent work functions and catalytic activity, and the LSPR effects of Au nanoparticles necessitate the importance to control the Au particle size. The Au size determines the extent of visible light absorption, catalytic sites and the nature of electron's behaviour (supply or reservoir). A control over Au size after the deposition is highly dependent on deposition methods and calcination conditions. Additionally, the Au loading must be optimised to maximise the rate of H_2O_2 formation, and reduce the blocking of light absorption on photocatalysts and rate of H_2O_2 decomposition.

3) **Choice of photocatalytic supports**. Besides the band positions that are suitable for H_2O_2 formation, the type of photocatalytic supports determines the contact structure as mentioned above. The surface properties e.g. acidity/basicity, functionality, of photocatalysts dictate the loading, coverage and dispersion of Au nanoparticles, and eventually aggregation and Au particle size. Moreover, the type of photocatalysts also affects the adsorption and rate of decomposition of H_2O_2 [88].

There is a plenty of room for further research and exploration to advance the progress of Au photocatalysis in H_2O_2 production. Herein we offer some perspective for future direction in this field. Firstly, the precise active site for O_2 adsorption and reduction is ambiguous; it could potentially be on an Au nanoparticle, at the interface between Au nanoparticle and the support, or on the surface of the photocatalyst. Using DFT calculations and the Au_{10} cluster on $TiO_2(110)$ as a model, Thetford et al. showed that O_2 is adsorbed on Au_{10}, and the formation of H_2O_2 proceeds at the interface of Au/TiO_2 and its decomposition occurs on Au nanoparticles [89]. The role of perimeter interface has also been found in other reactions [90]. Similarly, the exact site for the decomposition of H_2O_2 is still unclear. Different decomposition pathways demand different strategic designs of Au photocatalysts.

Secondly, a wide Au particle size distribution i.e., size polydispersity, impedes a precise identification of the catalytic active sites and the role of size-specific Au nanoparticles. Additionally, the aggregation of Au nanoparticles on supports might conceal the true nature of the catalytic active sites. Several approaches to prepare highly stable and resistant Au

catalysts against sintering have been reported such as the use of porous supports, transformation of supports, epitaxial overgrowth, overlayer coating, and encapsulation of Au nanoparticles in the porous support cavity [62,91–94]. An alternative is to explore atomically-precise Au clusters with definite size and structure and/or single Au atom catalysts [95–99].

Thirdly, the photocatalyst stability and poisoning needs further investigations. In the case of surface modification of photocatalysts with ions to boost the photocatalytic activity, it is unclear how these ions affect the stability or poisoning of Au nanoparticles. Understanding the poisoning mechanism might offer strategies for recycling Au photocatalysts for a long-term use.

Although this review presents discussion exclusively about photocatalytic H_2O_2 generation, it has prospect for other related practical applications. While the large-scale production and high concentration (30-70 wt%) of H_2O_2 are required for commercial purposes, small-scale and diluted H_2O_2 (0.1-1 wt%) that can be produced on-site is potentially useful for advanced oxidation process (AOP) and environmental remediation such as Fenton reaction [100]. For example, Xing et al. showed that the degradation of rhodamine B by a photocatalytic-assisted Fenton reaction at low H_2O_2 concentration superseded the traditional Fenton reaction by 18.5 folds and reduced the chemical oxygen demand (COD) by 96.5% [101]. It can be anticipated that Au photocatalysts will their place in wastewater treatment.

A study by Roy et al. discovered that micromolar H_2O_2 concentrations facilitated wound healing while high concentrations (≥3%) cause inflammatory and tissue damage [3]. Au photocatalysts can be used and integrated into microfluidic devices equipped with a UV LED for remote, on-site H_2O_2 generation which would greatly benefit the medical sector. Such devices must be able to produce the exact low concentration of H_2O_2 which can be applied on the surface of wound sites for healing process.

For some applications that utilize H_2O_2 as oxidant such as oxidation of alcohols, amines or epoxidation, H_2O_2 must be activated immediately for further use [102,103]. It seems counterintuitive to discuss about decomposition of H_2O_2 in this article yet as a stoichiometric oxidant, the photocatalytic activity depends on how much H_2O_2 is formed, activated, and then decomposes. Tada and co-workers found that the catalytic activity in cinnamyl alcohol oxidation corresponded to the rate of H_2O_2 decomposition over Au/TiO_2 and $Au/SrTiO_3$ [54,88]. While these works still required adding H_2O_2 as an oxidant, they offer a prospect for

future work without the need for external H_2O_2 in photocatalytic organic transformation by utilizing in situ generation of H_2O_2 using gold photocatalysts.

In the last decade, H_2O_2 has become an attractive alternative fuel and energy carrier to H_2. Its maximum theoretical potential is 1.09 V, which is reasonably close to H_2 fuel cells [104]. Simultaneous photocatalytic generation of H_2O_2 and H_2 is desirable for the use in fuel cells because it eliminates the use of membrane separation of liquid H_2O_2 and gaseous H_2. Wang et al. recently demonstrated a simultaneous H_2 and H_2O_2 generation up to 7.41 and 5.10 mmol $g^{-1} h^{-1}$, respectively, using Pt/TiO_2(anatase) [105]. It is timely to investigate the performance of Au photocatalysts in simultaneous production of H_2 and H_2O_2 and compare with other photocatalytic materials for screening purposes.

While the prospects of practical applications of photocatalytic H_2O_2 generation are appealing and promising, further research should be dedicated to addressing the fundamental issues, improving the photocatalytic efficiency and meeting the criteria for achieving practical utility. Gold photocatalysts can be a material of choice to stimulate further research in this multifaceted area. We believe this timely review is a starting point for this purpose.

Acknowledgement

References

[1] C. Samanta, Direct synthesis of hydrogen peroxide from hydrogen and oxygen: An overview of recent developments in the process, Applied Catalysis A: General. 350 (2008) 133–149. https://doi.org/10.1016/j.apcata.2008.07.043.

[2] J.M. Campos-Martin, G. Blanco-Brieva, J.L.G. Fierro, Hydrogen Peroxide Synthesis: An Outlook beyond the Anthraquinone Process, Angewandte Chemie International Edition. 45 (2006) 6962–6984. https://doi.org/10.1002/anie.200503779.

[3] S. Roy, S. Khanna, K. Nallu, T.K. Hunt, C.K. Sen, Dermal Wound Healing Is Subject to Redox Control, Molecular Therapy. 13 (2006) 211–220. https://doi.org/10.1016/j.ymthe.2005.07.684.

[4] R.S. Arnold, J. Shi, E. Murad, A.M. Whalen, C.Q. Sun, R. Polavarapu, S. Parthasarathy, J.A. Petros, J.D. Lambeth, Hydrogen peroxide mediates the cell growth and transformation caused by the mitogenic oxidase Nox1, Proceedings of the National Academy of Sciences. 98 (2001) 5550–5555. https://doi.org/10.1073/pnas.101505898.

[5] Q. Chen, Development of an anthraquinone process for the production of hydrogen peroxide in a trickle bed reactor—From bench scale to industrial scale, Chemical Engineering and Processing: Process Intensification. 47 (2008) 787–792. https://doi.org/10.1016/j.cep.2006.12.012.

[6] T. Nishimi, T. Kamachi, K. Kato, T. Kato, K. Yoshizawa, Mechanistic Study on the Production of Hydrogen Peroxide in the Anthraquinone Process, European Journal of Organic Chemistry. 2011 (2011) 4113–4120. https://doi.org/10.1002/ejoc.201100300.

[7] S. Wu, X. Quan, Design Principles and Strategies of Photocatalytic H2O2 Production from O2 Reduction, ACS EST Eng. 2 (2022) 1068–1079. https://doi.org/10.1021/acsestengg.1c00456.

[8] H. Song, L. Wei, L. Chen, H. Zhang, J. Su, Photocatalytic Production of Hydrogen Peroxide over Modified Semiconductor Materials: A Minireview, Topics in Catalysis. 63 (2020) 895–912. https://doi.org/10.1007/s11244-020-01317-9.

[9] L. Wang, J. Zhang, Y. Zhang, H. Yu, Y. Qu, J. Yu, Inorganic Metal-Oxide Photocatalyst for H2O2 Production, Small. 18 (2022) 2104561. https://doi.org/10.1002/smll.202104561.

[10] S. Goldstein, D. Aschengrau, Y. Diamant, J. Rabani, Photolysis of Aqueous H2O2: Quantum Yield and Applications for Polychromatic UV Actinometry in Photoreactors, Environ. Sci. Technol. 41 (2007) 7486–7490. https://doi.org/10.1021/es071379t.

[11] G.J. Hutchings, M. Haruta, A golden age of catalysis: A perspective, Applied Catalysis A: General. 291 (2005) 2–5. https://doi.org/10.1016/j.apcata.2005.05.044.

[12] T. Ishida, T. Murayama, A. Taketoshi, M. Haruta, Importance of Size and Contact Structure of Gold Nanoparticles for the Genesis of Unique Catalytic Processes, Chem. Rev. 120 (2020) 464–525. https://doi.org/10.1021/acs.chemrev.9b00551.

[13] P. Landon, P.J. Collier, A.J. Papworth, C.J. Kiely, G.J. Hutchings, Direct formation of hydrogen peroxide from H2/O2 using a gold catalyst, Chem. Commun. (2002) 2058–2059. https://doi.org/10.1039/B205248M.

[14] J.K. Edwards, B.E. Solsona, P. Landon, A.F. Carley, A. Herzing, C.J. Kiely, G.J. Hutchings, Direct synthesis of hydrogen peroxide from H2 and O2 using TiO2-supported Au–Pd catalysts, Journal of Catalysis. 236 (2005) 69–79. https://doi.org/10.1016/j.jcat.2005.09.015.

[15] M. Teranishi, S. Naya, H. Tada, In Situ Liquid Phase Synthesis of Hydrogen Peroxide from Molecular Oxygen Using Gold Nanoparticle-Loaded Titanium(IV) Dioxide Photocatalyst, J. Am. Chem. Soc. 132 (2010) 7850–7851. https://doi.org/10.1021/ja102651g.

[16] K. Fuku, Y. Miyase, Y. Miseki, T. Funaki, T. Gunji, K. Sayama, Photoelectrochemical Hydrogen Peroxide Production from Water on a WO3/BiVO4 Photoanode and from O2 on an Au Cathode Without External Bias, Chemistry – An Asian Journal. 12 (2017) 1111–1119. https://doi.org/10.1002/asia.201700292.

[17] Y. Wang, Y. Wang, J. Zhao, M. Chen, X. Huang, Y. Xu, Efficient production of H2O2 on Au/WO3 under visible light and the influencing factors, Applied Catalysis B: Environmental. 284 (2021) 119691. https://doi.org/10.1016/j.apcatb.2020.119691.

[18] K. Kim, J. Park, H. Kim, G.Y. Jung, M.-G. Kim, Solid-Phase Photocatalysts: Physical Vapor Deposition of Au Nanoislands on Porous TiO2 Films for Millimolar H2O2 Production within a Few Minutes, ACS Catal. 9 (2019) 9206–9211. https://doi.org/10.1021/acscatal.9b02269.

[19] C. Wang, D. Astruc, Nanogold plasmonic photocatalysis for organic synthesis and clean energy conversion, Chem. Soc. Rev. 43 (2014) 7188–7216. https://doi.org/10.1039/C4CS00145A.

[20] H. Zhu, X. Yuan, Q. Yao, J. Xie, Shining photocatalysis by gold-based nanomaterials, Nano Energy. 88 (2021) 106306. https://doi.org/10.1016/j.nanoen.2021.106306.

[21] C.-L. Tan, F. Zhang, Y.-H. Li, Z.-R. Tang, Y.-J. Xu, Au clusters-based visible light photocatalysis, Research on Chemical Intermediates. 47 (2021) 29–50. https://doi.org/10.1007/s11164-020-04346-x.

[22] M. Teranishi, S. Naya, H. Tada, Temperature- and pH-Dependence of Hydrogen Peroxide Formation from Molecular Oxygen by Gold Nanoparticle-Loaded Titanium(IV) Oxide Photocatalyst, J. Phys. Chem. C. 120 (2016) 1083–1088. https://doi.org/10.1021/acs.jpcc.5b10626.

[23] M. Teranishi, R. Hoshino, S. Naya, H. Tada, Gold-Nanoparticle-Loaded Carbonate-Modified Titanium(IV) Oxide Surface: Visible-Light-Driven Formation of Hydrogen Peroxide from Oxygen, Angewandte Chemie International Edition. 55 (2016) 12773–12777. https://doi.org/10.1002/anie.201606734.

[24] X. Xiong, X. Zhang, S. Liu, J. Zhao, Y. Xu, Sustained production of H2O2 in alkaline water solution using borate and phosphate-modified Au/TiO2 photocatalysts, Photochemical & Photobiological Sciences. 17 (2018) 1018–1022. https://doi.org/10.1039/c8pp00177d.

[25] Z. Liu, X. Sheng, D. Wang, X. Feng, Efficient Hydrogen Peroxide Generation Utilizing Photocatalytic Oxygen Reduction at a Triphase Interface, IScience. 17 (2019) 67–73. https://doi.org/10.1016/j.isci.2019.06.023.

[26] W. Xu, X. Sheng, H. Zhou, D. Wang, Z. Ding, X. Feng, Enhanced plasmonic photocatalytic synthesis of hydrogen peroxide at an air-liquid-solid triphasic interface, Chemical Engineering Journal. 410 (2021) 128342. https://doi.org/10.1016/j.cej.2020.128342.

[27] L. Li, B. Li, L. Feng, X. Zhang, Y. Zhang, Q. Zhao, G. Zuo, X. Meng, Au Modified F-TiO2 for Efficient Photocatalytic Synthesis of Hydrogen Peroxide, Molecules. 26 (2021). https://doi.org/10.3390/molecules26133844.

[28] Y. Wang, Y. Wang, J. Zhao, Y. Xu, Effect of inorganic ions on H2O2 production over illuminated Au/WO3 with visible light, Applied Catalysis B: Environmental. 299 (2021) 120676. https://doi.org/10.1016/j.apcatb.2021.120676.

[29] S. Kawano, M. Fujishima, H. Tada, Size effect of zinc oxide-supported gold nanoparticles on the photocatalytic activity for two-electron oxygen reduction reaction, Catalysis Communications. 144 (2020) 106076. https://doi.org/10.1016/j.catcom.2020.106076.

[30] X. Meng, P. Zong, L. Wang, F. Yang, W. Hou, S. Zhang, B. Li, Z. Guo, S. Liu, G. Zuo, Y. Du, T. Wang, V.A.L. Roy, Au-nanoparticle-supported ZnO as highly efficient photocatalyst for H2O2 production, Catalysis Communications. 134 (2020) 105860. https://doi.org/10.1016/j.catcom.2019.105860.

[31] H. Song, L. Wei, C. Chen, C. Wen, F. Han, Photocatalytic production of H2O2 and its in situ utilization over atomic-scale Au modified MoS2 nanosheets, Journal of Catalysis. 376 (2019) 198–208. https://doi.org/10.1016/j.jcat.2019.06.015.

[32] H. Hirakawa, S. Shiota, Y. Shiraishi, H. Sakamoto, S. Ichikawa, T. Hirai, Au Nanoparticles Supported on BiVO4: Effective Inorganic Photocatalysts for H2O2 Production from Water and O2 under Visible Light, ACS Catal. 6 (2016) 4976–4982. https://doi.org/10.1021/acscatal.6b01187.

[33] R. An, Y. Zhao, H. Bai, L. Wang, C. Li, Decoration of Au NPs on hollow structured BiOBr with surface oxygen vacancies for enhanced visible light photocatalytic H2O2 evolution, Journal of Solid State Chemistry. 306 (2022) 122722. https://doi.org/10.1016/j.jssc.2021.122722.

[34] G. Zuo, S. Liu, L. Wang, H. Song, P. Zong, W. Hou, B. Li, Z. Guo, X. Meng, Y. Du, T. Wang, V.A.L. Roy, Finely dispersed Au nanoparticles on graphitic carbon nitride as highly active photocatalyst for hydrogen peroxide production, Catalysis Communications. 123 (2019) 69–72. https://doi.org/10.1016/j.catcom.2019.02.011.

[35] X. Chang, J. Yang, D. Han, B. Zhang, X. Xiang, J. He, Enhancing Light-Driven Production of Hydrogen Peroxide by Anchoring Au onto C3N4 Catalysts, Catalysts. 8 (2018). https://doi.org/10.3390/catal8040147.

[36] S. Jiang, C. Xiong, S. Song, B. Cheng, Plasmonic Graphene-Like Au/C3N4 Nanosheets with Barrier-Free Interface for Photocatalytically Sustainable Evolution of Active Oxygen Species, ACS Sustainable Chem. Eng. 7 (2019) 2018–2026. https://doi.org/10.1021/acssuschemeng.8b04338.

[37] J. Liang, Y. Liu, Z. Si, G. Wei, D. Weng, F. Kang, Graphene quantum dots piecing together into graphene on nano Au for overall water splitting, Carbon. 178 (2021) 265–272. https://doi.org/10.1016/j.carbon.2021.02.100.

[38] H. Shi, Y. Li, X. Wang, H. Yu, J. Yu, Selective modification of ultra-thin g-C3N4 nanosheets on the (110) facet of Au/BiVO4 for boosting photocatalytic H2O2 production, Applied Catalysis B: Environmental. 297 (2021) 120414. https://doi.org/10.1016/j.apcatb.2021.120414.

[39] L. Feng, B. Li, Y. Xiao, L. Li, Y. Zhang, Q. Zhao, G. Zuo, X. Meng, V.A.L. Roy, Au modified Bi2O3-TiO2 hybrid for photocatalytic synthesis of hydrogen peroxide, Catalysis Communications. 155 (2021) 106315. https://doi.org/10.1016/j.catcom.2021.106315.

[40] K. Awa, S. Naya, M. Fujishima, H. Tada, A Three-Component Plasmonic Photocatalyst Consisting of Gold Nanoparticle and TiO2–SnO2 Nanohybrid with Heteroepitaxial Junction: Hydrogen Peroxide Synthesis, J. Phys. Chem. C. 124 (2020) 7797–7802. https://doi.org/10.1021/acs.jpcc.9b11875.

[41] M. Nagamitsu, K. Awa, H. Tada, Hydrogen peroxide synthesis from water and oxygen using a three-component nanohybrid photocatalyst consisting of Au particle-loaded

rutile TiO2 and RuO2 with a heteroepitaxial junction, Chem. Commun. 56 (2020) 8190–8193. https://doi.org/10.1039/D0CC03327H.

[42] D. Tsukamoto, A. Shiro, Y. Shiraishi, Y. Sugano, S. Ichikawa, S. Tanaka, T. Hirai, Photocatalytic H2O2 Production from Ethanol/O2 System Using TiO2 Loaded with Au–Ag Bimetallic Alloy Nanoparticles, ACS Catal. 2 (2012) 599–603. https://doi.org/10.1021/cs2006873.

[43] X. Pang, N. Skillen, D.W. Bahnemann, D.W. Rooney, P.K.J. Robertson, Photocatalytic H2O2 Generation Using Au-Ag Bimetallic Alloy Nanoparticles loaded on ZnO, Catalysts. 12 (2022). https://doi.org/10.3390/catal12090939.

[44] K. Wang, M. Wang, J. Yu, D. Liao, H. Shi, X. Wang, H. Yu, BiVO4 Microparticles Decorated with Cu@Au Core-Shell Nanostructures for Photocatalytic H2O2 Production, ACS Appl. Nano Mater. 4 (2021) 13158–13166. https://doi.org/10.1021/acsanm.1c02688.

[45] J. Cao, J. Cai, R. Li, J.H. Han, J. Liu, M. Huang, A Novel 3D Yolk–Double-Shell Au@CdS/g-C3N4 Nanostructure with Enhanced Photoelectrochemical and Photocatalytic Properties, J. Phys. Chem. C. 126 (2022) 4939–4947. https://doi.org/10.1021/acs.jpcc.1c09841.

[46] H. Shi, Y. Li, K. Wang, S. Li, X. Wang, P. Wang, F. Chen, H. Yu, Mass-transfer control for selective deposition of well-dispersed AuPd cocatalysts to boost photocatalytic H2O2 production of BiVO4, Chemical Engineering Journal. 443 (2022) 136429. https://doi.org/10.1016/j.cej.2022.136429.

[47] N. Kaynan, B.A. Berke, O. Hazut, R. Yerushalmi, Sustainable photocatalytic production of hydrogen peroxide from water and molecular oxygen, J. Mater. Chem. A. 2 (2014) 13822–13826. https://doi.org/10.1039/C4TA03004D.

[48] D.E. Willis, M.M. Taheri, O. Kizilkaya, T.R. Leite, L. Zhang, T. Ofoegbuna, K. Ding, J.A. Dorman, J.B. Baxter, K.M. McPeak, Critical Coupling of Visible Light Extends Hot-Electron Lifetimes for H2O2 Synthesis, ACS Appl. Mater. Interfaces. 12 (2020) 22778–22788. https://doi.org/10.1021/acsami.0c00825.

[49] S. Mansingh, D.P. Sahoo, L. Paramanik, M. Sahoo, K. Parida, Robust charge carrier engineering via plasmonic effect and conjugated Π-framework on Au loaded ZnCr-LDH/RGO photocatalyst towards H2 and H2O2 production, Inorg. Chem. Front. 9 (2022) 559–576. https://doi.org/10.1039/D1QI01284C.

[50] Q. Xue, Z. Wang, S. Han, Y. Liu, X. Dou, Y. Li, H. Zhu, X. Yuan, Ligand engineering of Au nanoclusters with multifunctional metalloporphyrins for photocatalytic H2O2 production, J. Mater. Chem. A. 10 (2022) 8371–8377. https://doi.org/10.1039/D2TA00720G.

[51] K.Y. Ho, K.L. Yeung, Properties of TiO2 support and the performance of Au/TiO2 Catalyst for CO oxidation reaction, Gold Bulletin. 40 (2007) 15–30. https://doi.org/10.1007/BF03215288.

[52] M. Mrowetz, A. Villa, L. Prati, E. Selli, Effects of Au nanoparticles on TiO2 in the photocatalytic degradation of an azo dye, Gold Bulletin. 40 (2007) 154–160. https://doi.org/10.1007/BF03215573.

[53] S. Tsubota, M. Haruta, T. Kobayashi, A. Ueda, Y. Nakahara, Preparation of Highly Dispersed Gold on Titanium and Magnesium Oxide, in: G. Poncelet, P.A. Jacobs, P. Grange, B. Delmon (Eds.), Studies in Surface Science and Catalysis, Elsevier, 1991: pp. 695–704. https://doi.org/10.1016/S0167-2991(08)64634-0.

[54] T. Kiyonaga, Q. Jin, H. Kobayashi, H. Tada, Size-Dependence of Catalytic Activity of Gold Nanoparticles Loaded on Titanium (IV) Dioxide for Hydrogen Peroxide

Decomposition, ChemPhysChem. 10 (2009) 2935–2938.
https://doi.org/10.1002/cphc.200900596.

[55] M.V. Dozzi, L. Prati, P. Canton, E. Selli, Effects of gold nanoparticles deposition on the photocatalytic activity of titanium dioxide under visible light, Phys. Chem. Chem. Phys. 11 (2009) 7171–7180. https://doi.org/10.1039/B907317E.

[56] N. Dimitratos, A. Villa, C.L. Bianchi, L. Prati, M. Makkee, Gold on titania: Effect of preparation method in the liquid phase oxidation, Applied Catalysis A: General. 311 (2006) 185–192. https://doi.org/10.1016/j.apcata.2006.06.026.

[57] J.F.S. Fernando, M.P. Shortell, C.J. Noble, J.R. Harmer, E.A. Jaatinen, E.R. Waclawik, Controlling Au Photodeposition on Large ZnO Nanoparticles, ACS Appl. Mater. Interfaces. 8 (2016) 14271–14283. https://doi.org/10.1021/acsami.6b03128.

[58] Q. Li, C. Wu, K. Wang, X. Wang, X. Chen, W. Dai, X. Fu, Comparison of the catalytic performance of Au/TiO2 prepared by in situ photodeposition and deposition precipitation methods for CO oxidation at room temperature under visible light irradiation, Catal. Sci. Technol. 12 (2022) 237–249. https://doi.org/10.1039/D1CY01829A.

[59] Y. Zhu, H. Qian, R. Jin, An Atomic-Level Strategy for Unraveling Gold Nanocatalysis from the Perspective of Aun(SR)m Nanoclusters, Chemistry – A European Journal. 16 (2010) 11455–11462. https://doi.org/10.1002/chem.201001086.

[60] D.P. Anderson, R.H. Adnan, J.F. Alvino, O. Shipper, B. Donoeva, J.-Y. Ruzicka, H. Al Qahtani, H.H. Harris, B. Cowie, J.B. Aitken, V.B. Golovko, G.F. Metha, G.G. Andersson, Chemically synthesised atomically precise gold clusters deposited and activated on titania. Part II, Phys. Chem. Chem. Phys. 15 (2013) 14806–14813. https://doi.org/10.1039/C3CP52497C.

[61] R.H. Adnan, V.B. Golovko, Benzyl Alcohol Oxidation Using Gold Catalysts Derived from Au8 Clusters on TiO2, Catalysis Letters. 149 (2019) 449–455. https://doi.org/10.1007/s10562-018-2625-8.

[62] A.S. Alotabi, D.J. Osborn, S. Ozaki, Y. Kataoka, Y. Negishi, S. Tesana, G.F. Metha, G.G. Andersson, Suppression of phosphine-protected Au9 cluster agglomeration on SrTiO3 particles using a chromium hydroxide layer, Mater. Adv. 3 (2022) 3620–3630. https://doi.org/10.1039/D1MA01226F.

[63] H.S. Al Qahtani, R. Higuchi, T. Sasaki, J.F. Alvino, G.F. Metha, V.B. Golovko, R. Adnan, G.G. Andersson, T. Nakayama, Grouping and aggregation of ligand protected Au9 clusters on TiO2 nanosheets, RSC Adv. 6 (2016) 110765–110774. https://doi.org/10.1039/C6RA21419C.

[64] A.S. Alotabi, Y. Yin, A. Redaa, S. Tesana, G.F. Metha, G.G. Andersson, Cr2O3 layer inhibits agglomeration of phosphine-protected Au9 clusters on TiO2 films, J. Chem. Phys. 155 (2021) 164702. https://doi.org/10.1063/5.0059912.

[65] X. Li, C. Chen, J. Zhao, Mechanism of Photodecomposition of H2O2 on TiO2 Surfaces under Visible Light Irradiation, Langmuir. 17 (2001) 4118–4122. https://doi.org/10.1021/la010035s.

[66] Y. Zhang, O. Pluchery, L. Caillard, A.-F. Lamic-Humblot, S. Casale, Y.J. Chabal, M. Salmeron, Sensing the Charge State of Single Gold Nanoparticles via Work Function Measurements, Nano Lett. 15 (2015) 51–55. https://doi.org/10.1021/nl503782s.

[67] N.T. Khoa, S.W. Kim, D.-H. Yoo, E.J. Kim, S.H. Hahn, Size-dependent work function and catalytic performance of gold nanoparticles decorated graphene oxide sheets, Applied Catalysis A: General. 469 (2014) 159–164. https://doi.org/10.1016/j.apcata.2013.08.046.

[68] S. Naya, T. Niwa, T. Kume, H. Tada, Visible-Light-Induced Electron Transport from Small to Large Nanoparticles in Bimodal Gold Nanoparticle-Loaded Titanium(IV) Oxide, Angewandte Chemie International Edition. 53 (2014) 7305–7309. https://doi.org/10.1002/anie.201402939.

[69] V. Jovic, W.-T. Chen, D. Sun-Waterhouse, M.G. Blackford, H. Idriss, G.I.N. Waterhouse, Effect of gold loading and TiO2 support composition on the activity of Au/TiO2 photocatalysts for H2 production from ethanol–water mixtures, Journal of Catalysis. 305 (2013) 307–317. https://doi.org/10.1016/j.jcat.2013.05.031.

[70] Tang Hailian, Su Yang, Zhang Bingsen, Lee Adam F., Isaacs Mark A., Wilson Karen, Li Lin, Ren Yuegong, Huang Jiahui, Haruta Masatake, Qiao Botao, Liu Xin, Jin Changzi, Su Dangsheng, Wang Junhu, Zhang Tao, Classical strong metal–support interactions between gold nanoparticles and titanium dioxide, Science Advances. 3 (2017) e1700231. https://doi.org/10.1126/sciadv.1700231.

[71] H. Wang, L. Wang, D. Lin, X. Feng, Y. Niu, B. Zhang, F.-S. Xiao, Strong metal–support interactions on gold nanoparticle catalysts achieved through Le Chatelier's principle, Nature Catalysis. 4 (2021) 418–424. https://doi.org/10.1038/s41929-021-00611-3.

[72] H. Tang, J. Wei, F. Liu, B. Qiao, X. Pan, L. Li, J. Liu, J. Wang, T. Zhang, Strong Metal–Support Interactions between Gold Nanoparticles and Nonoxides, J. Am. Chem. Soc. 138 (2016) 56–59. https://doi.org/10.1021/jacs.5b11306.

[73] B. Qiao, J.-X. Liang, A. Wang, C.-Q. Xu, J. Li, T. Zhang, J.J. Liu, Ultrastable single-atom gold catalysts with strong covalent metal-support interaction (CMSI), Nano Research. 8 (2015) 2913–2924. https://doi.org/10.1007/s12274-015-0796-9.

[74] S. Wang, B. Zeng, C. Li, Effects of Au nanoparticle size and metal-support interaction on plasmon-induced photocatalytic water oxidation, Chinese Journal of Catalysis. 39 (2018) 1219–1227. https://doi.org/10.1016/S1872-2067(18)63094-3.

[75] M. Ma, H. Wang, H. Liu, Steering spatially separated dual sites on nano-TiO2 through SMSI and lattice matching for robust photocatalytic hydrogen evolution, Chinese Chemical Letters. 32 (2021) 3613–3618. https://doi.org/10.1016/j.cclet.2021.04.012.

[76] Y. Liu, L. Chen, J. Hu, J. Li, R. Richards, TiO2 Nanoflakes Modified with Gold Nanoparticles as Photocatalysts with High Activity and Durability under near UV Irradiation, J. Phys. Chem. C. 114 (2010) 1641–1645. https://doi.org/10.1021/jp910500c.

[77] F. Xue, Y. Si, C. Cheng, W. Fu, X. Chen, S. Shen, L. Wang, M. Liu, Electron transfer via homogeneous phosphorus bridges enabling boosted photocatalytic generation of H2 and H2O2 from pure water with stoichiometric ratio, Nano Energy. 103 (2022) 107799. https://doi.org/10.1016/j.nanoen.2022.107799.

[78] Y. Liu, Y. Zhao, Y. Sun, J. Cao, H. Wang, X. Wang, H. Huang, M. Shao, Y. Liu, Z. Kang, A 4e-–2e- cascaded pathway for highly efficient production of H2 and H2O2 from water photo-splitting at normal pressure, Applied Catalysis B: Environmental. 270 (2020) 118875. https://doi.org/10.1016/j.apcatb.2020.118875.

[79] F. Xue, Y. Si, M. Wang, M. Liu, L. Guo, Toward efficient photocatalytic pure water splitting for simultaneous H2 and H2O2 production, Nano Energy. 62 (2019) 823–831. https://doi.org/10.1016/j.nanoen.2019.05.086.

[80] A.W. Phillips, R. Parameswaran, E. Lichter, J. Jeong, L. Meng, M. Burke, K. Koehler, Y.V. Lee, B. Tian, Gold-Decorated Silicon Nanowire Photocatalysts for Intracellular Production of Hydrogen Peroxide, ACS Appl. Mater. Interfaces. 13 (2021) 15490–15500. https://doi.org/10.1021/acsami.0c23164.

[81] N. Waiskopf, Y. Ben-Shahar, M. Galchenko, I. Carmel, G. Moshitzky, H. Soreq, U. Banin, Photocatalytic Reactive Oxygen Species Formation by Semiconductor–Metal Hybrid Nanoparticles. Toward Light-Induced Modulation of Biological Processes, Nano Lett. 16 (2016) 4266–4273. https://doi.org/10.1021/acs.nanolett.6b01298.

[82] H. Kobayashi, M. Teranishi, R. Negishi, S. Naya, H. Tada, Reaction Mechanism of the Multiple-Electron Oxygen Reduction Reaction on the Surfaces of Gold and Platinum Nanoparticles Loaded on Titanium(IV) Oxide, J. Phys. Chem. Lett. 7 (2016) 5002–5007. https://doi.org/10.1021/acs.jpclett.6b02026.

[83] Y. Liu, Z. Sun, Y.H. Hu, Bimetallic cocatalysts for photocatalytic hydrogen production from water, Chemical Engineering Journal. 409 (2021) 128250. https://doi.org/10.1016/j.cej.2020.128250.

[84] E.M. Goliaei, N. Seriani, Structure and Electronic Properties of Small Silver–Gold Clusters on Titania Photocatalysts for H2O2 Production: An Investigation with Density Functional Theory, J. Phys. Chem. C. 123 (2019) 2855–2863. https://doi.org/10.1021/acs.jpcc.8b09300.

[85] Y. Shiraishi, S. Kanazawa, D. Tsukamoto, A. Shiro, Y. Sugano, T. Hirai, Selective Hydrogen Peroxide Formation by Titanium Dioxide Photocatalysis with Benzylic Alcohols and Molecular Oxygen in Water, ACS Catal. 3 (2013) 2222–2227. https://doi.org/10.1021/cs400511q.

[86] J. Zhang, L. Zheng, F. Wang, C. Chen, H. Wu, S.A.K. Leghari, M. Long, The critical role of furfural alcohol in photocatalytic H2O2 production on TiO2, Applied Catalysis B: Environmental. 269 (2020) 118770. https://doi.org/10.1016/j.apcatb.2020.118770.

[87] V. Maurino, C. Minero, G. Mariella, E. Pelizzetti, Sustained production of H2O2 on irradiated TiO2 – fluoride systems, Chem. Commun. (2005) 2627–2629. https://doi.org/10.1039/B418789J.

[88] S. Naya, M. Teranishi, K. Kimura, H. Tada, A strong support-effect on the catalytic activity of gold nanoparticles for hydrogen peroxide decomposition, Chem. Commun. 47 (2011) 3230–3232. https://doi.org/10.1039/C0CC03047C.

[89] A. Thetford, G.J. Hutchings, S.H. Taylor, D.J. Willock, The decomposition of H2O2 over the components of Au/TiO2 catalysts, Proceedings of the Royal Society A: Mathematical, Physical and Engineering Sciences. 467 (2011) 1885–1899. https://doi.org/10.1098/rspa.2010.0561.

[90] M. Haruta, Spiers Memorial Lecture Role of perimeter interfaces in catalysis by gold nanoparticles, Faraday Discuss. 152 (2011) 11–32. https://doi.org/10.1039/C1FD00107H.

[91] S. Wang, Q. Zhao, H. Wei, J.-Q. Wang, M. Cho, H.S. Cho, O. Terasaki, Y. Wan, Aggregation-Free Gold Nanoparticles in Ordered Mesoporous Carbons: Toward Highly Active and Stable Heterogeneous Catalysts, J. Am. Chem. Soc. 135 (2013) 11849–11860. https://doi.org/10.1021/ja403822d.

[92] L. Wang, J. Zhang, Y. Zhu, S. Xu, C. Wang, C. Bian, X. Meng, F.-S. Xiao, Strong Metal–Support Interactions Achieved by Hydroxide-to-Oxide Support Transformation for Preparation of Sinter-Resistant Gold Nanoparticle Catalysts, ACS Catal. 7 (2017) 7461–7465. https://doi.org/10.1021/acscatal.7b01947.

[93] S. Liu, W. Xu, W. Liu, L. Li, J. Wang, Sintering-resistant Au/iron oxide-hydroxyapatite nanocatalysts achieved by tuning strong metal-support interactions, Catalysis Today. 382 (2021) 13–21. https://doi.org/10.1016/j.cattod.2021.01.012.

[94] J. Fang, Y. Zhang, Y. Zhou, S. Zhao, C. Zhang, H. Zhang, X. Sheng, K. Wang, Fabrication of Ellipsoidal Silica Yolk–Shell Magnetic Structures with Extremely Stable Au

Nanoparticles as Highly Reactive and Recoverable Catalysts, Langmuir. 33 (2017) 2698–2708. https://doi.org/10.1021/acs.langmuir.6b03873.

[95] T. Higaki, Y. Li, S. Zhao, Q. Li, S. Li, X.-S. Du, S. Yang, J. Chai, R. Jin, Atomically Tailored Gold Nanoclusters for Catalytic Application, Angewandte Chemie International Edition. 58 (2019) 8291–8302. https://doi.org/10.1002/anie.201814156.

[96] R. Jin, G. Li, S. Sharma, Y. Li, X. Du, Toward Active-Site Tailoring in Heterogeneous Catalysis by Atomically Precise Metal Nanoclusters with Crystallographic Structures, Chem. Rev. 121 (2021) 567–648. https://doi.org/10.1021/acs.chemrev.0c00495.

[97] R.H. Adnan, J.M.L. Madridejos, A.S. Alotabi, G.F. Metha, G.G. Andersson, A Review of State of the Art in Phosphine Ligated Gold Clusters and Application in Catalysis, Advanced Science. 9 (2022) 2105692. https://doi.org/10.1002/advs.202105692.

[98] C. Gao, J. Low, R. Long, T. Kong, J. Zhu, Y. Xiong, Heterogeneous Single-Atom Photocatalysts: Fundamentals and Applications, Chem. Rev. 120 (2020) 12175–12216. https://doi.org/10.1021/acs.chemrev.9b00840.

[99] Y. Xia, M. Sayed, L. Zhang, B. Cheng, J. Yu, Single-atom heterogeneous photocatalysts, Chem Catalysis. 1 (2021) 1173–1214. https://doi.org/10.1016/j.checat.2021.08.009.

[100] W. Shi, W. Sun, Y. Liu, K. Zhang, H. Sun, X. Lin, Y. Hong, F. Guo, A self-sufficient photo-Fenton system with coupling in-situ production H2O2 of ultrathin porous g-C3N4 nanosheets and amorphous FeOOH quantum dots, Journal of Hazardous Materials. 436 (2022) 129141. https://doi.org/10.1016/j.jhazmat.2022.129141.

[101] M. Xing, W. Xu, C. Dong, Y. Bai, J. Zeng, Y. Zhou, J. Zhang, Y. Yin, Metal Sulfides as Excellent Co-catalysts for H2O2 Decomposition in Advanced Oxidation Processes, Chem. 4 (2018) 1359–1372. https://doi.org/10.1016/j.chempr.2018.03.002.

[102] K. Kurokawa, H. Sugime, S. Naya, H. Tada, Thermocatalytic Activity of Gold Truncated Nanopyramids on Strontium Titanate Nanocube, Chem. Lett. 50 (2021) 1997–2000. https://doi.org/10.1246/cl.210544.

[103] A. Graml, B. König, Synthesis of anti-Markovnikov Alcohols via Epoxidation and Hydrogenation of Styrenes using Photocatalytically Generated Redox Equivalents, ChemPhotoChem. 5 (2021) 362–368. https://doi.org/10.1002/cptc.202000205.

[104] C.J. McDonnell-Worth, D.R. MacFarlane, Progress Towards Direct Hydrogen Peroxide Fuel Cells (DHPFCs) as an Energy Storage Concept*, Aust. J. Chem. 71 (2018) 781–788.

[105] L. Wang, S. Cao, K. Guo, Z. Wu, Z. Ma, L. Piao, Simultaneous hydrogen and peroxide production by photocatalytic water splitting, Chinese Journal of Catalysis. 40 (2019) 470–475. https://doi.org/10.1016/S1872-2067(19)63274-2.